ADVANCED ENERGY MATERIALS
www.advenergymat.de

Quantum Dots for Photovoltaics: A Tale of Two Materials

Leiping Duan, Long Hu, Xinwei Guan, Chun-Ho Lin, Dewei Chu, Shujuan Huang, Xiaogang Liu, Jianyu Yuan,* and Tom Wu**

Quantum dot (QD) solar cells, benefiting from unique quantum confinement effects and multiple exciton generation, have attracted great research attention in the past decades. Before 2016, research efforts were mainly devoted to solar cells comprising lead chalcogenide QDs, while lead halide perovskite QDs have recently emerged as a rising star in the field. This review aims to compare similarities and differences between lead chalcogenide and lead halide perovskite QDs for photovoltaic applications. The fundamental physical properties of these two types of nanomaterials and their state-of-the-art photovoltaic devices are summarized, with a focus on ligand and device engineering. Furthermore, a special section is devoted to the stability issue that often hinders photovoltaic technologies. Finally, future development in tandem devices, challenges associated with large-size cell fabrication and lead toxicity, and potential mitigation solutions are discussed.

1. Introduction

Owing to the ever-increasing demand for energy and exacerbating environmental issues resulting from fossil fuel combustion, securing sustainable and clean energy technologies has become a paramount task in the 21st century. Photovoltaic (PV) devices, converting solar energy to electrical energy, have drawn much attention. Current commercialized PV technologies mainly rely on crystalline silicon (Si) devices, which have approached theoretical maximum efficiency.[1,2] Therefore, new PV technologies such as, organic solar cells (OSCs), perovskite solar cells (PSCs), and colloidal quantum dots (QDs) solar cells, have been quickly developed.[3–11] Among these diverse PV materials, QDs possess unique nanostructural uniformity and highly tunable features, including quantum confinement effects and multiple exciton generation (MEG).[12–17] QD solar cells can be fabricated as semitransparent and flexible for promising applications, such as, wearable energy collectors and building-integrated photovoltaics.[18,19]

QDs are defined as nanometer-sized semiconducting crystals, usually chemically synthesized with surface ligands.[20,21] When the size of a semiconducting crystal reduces to the molecular scale, its bulk properties alter simultaneously.[22,23] Owing to the quantum confinement effect, the absorption spectra and energy levels of QDs can be easily tuned by size variation. For example, the bandgap of cadmium telluride (CdTe) bulk material is around 1.48 eV, while the bandgap of the CdTe QD can be tuned from 2.06 to 2.32 eV by a slight size reduction from 2.47 to 2.10 nm.[24,25] The quantum confinement effect also allows better energy level and absorption matching for QD-based optoelectronic devices such as photodetectors, light-emitting diodes, and solar cells.[26–34] Additionally, QDs enable hot cattier extraction due to the MEG effect, where one absorbed photon with high energy may generate two or more excitons.[27,35,36] The unique capability of MEG in QD solar cells can potentially improve the power conversion efficiency (PCE) of single-junction devices and thus overcome the Shockley–Queisser (SQ) PCE limit.[37–39]

In the past decades, increasing research attention has been paid to QD solar cells, and many materials have been exploited in this context. Although there have been some trials on lead-free materials, such as Indium arsenide (InAs), InP, and $AgBiS_2$, their device performances are still poor, with PCE less than 6%.[40–45] Up to now, most of the high-performance devices were reported from lead-based QDs in two main categories: lead chalcogenides (PbX, X = S, Se) and lead halide perovskites (PVK). **Figure 1**a depicts the progress in PCE values and accumulated publication numbers of lead-based QD solar cells, shown as points and columns, respectively, since 2010. With recent progress in device structure design, band-alignment engineering, and optimized surface passivation, the PCE of QD solar cells has constantly increased, achieving a record of 16.6% to date.[46–48]

Before 2016, QD solar cells were mainly composed of PbX (X = S, Se), and continuous efforts have recently culminated in a remarkable PCE of 13.8%.[53–55] PbX usually crystallizes in a cubic structure with S or Se atoms located at octahedral

Dr. L. Duan, Dr. L. Hu, X. Guan, Dr. C.-H. Lin, Prof. D. Chu, Prof. T. Wu
School of Material Science and Engineering
University of New South Wales
Sydney, NSW 2052, Australia
E-mail: long.hu@unsw.edu.au; tom.wu@unsw.edu.au
Dr. L. Hu, Prof. S. Huang
School of Engineering
Macquarie University Sustainable Energy Research Centre
Macquarie University
Sydney, NSW 2109, Australia
Prof. X. Liu
Department of Chemistry
National University of Singapore
Singapore 117596, Singapore
Prof. J. Yuan
Institute of Functional Nano & Soft Materials (FUNSOM)
Jiangsu Key Laboratory for Carbon-Based Functional Materials and Devices
Soochow University
Suzhou, Jiangsu 215123, China
E-mail: jyyuan@suda.edu.cn
The ORCID identification number(s) for the author(s) of this article can be found under https://doi.org/10.1002/aenm.202100354.

DOI: 10.1002/aenm.202100354

 © 2021 Wiley-VCH GmbH

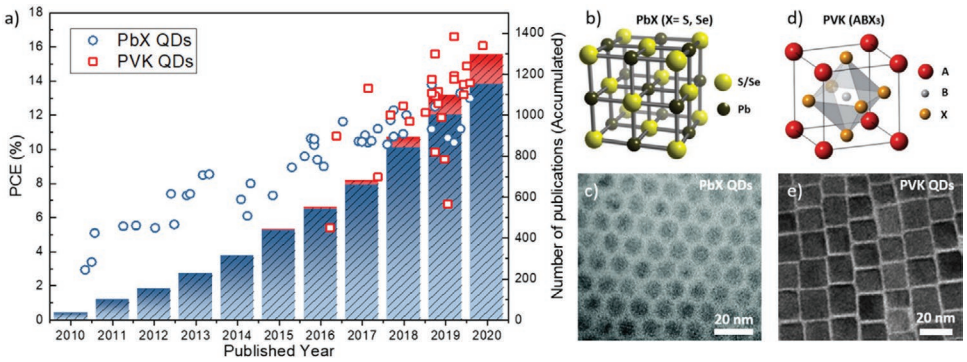

Figure 1. a) Progress in the PCE and the accumulated publication numbers of lead-based QD solar cells since 2010.[88–148] The data of the number of publications is taken from Scopus (www.scopus.com). b) Schematic diagram of the material structure of PbX (X = S, Se) (Reproduced with permission.[49] Copyright 2018, Shichen Yin). c) The transmission electron microscope (TEM) image of PbS QDs (Reproduced with permission.[50] Copyright 2015, The Royal Society of Chemistry). d) Schematic diagram of the material structure of PVK (ABX_3) (Reproduced with permission.[51] Copyright 2014, The Royal Society of Chemistry). e) The TEM image of $CsPbBr_3$ QDs (Reproduced with permission.[52] Copyright 2017, The Royal Society of Chemistry).

interstices of the face-centered sub-lattice of Pb atoms (Figure 1b).[11,56,57] In general, the QD shape is dependent on the size and growth kinetics. According to the Wulff construction theory, the ratio between surface energies of (111) and (100) lattice planes leads to the equilibrium shape of PbX QDs.[58] PbS QDs with a size greater than 4.74 nm exhibit a cuboctahedron shape with truncated (100) facets (Figure 1c).[50] QDs with tunable sizes offer tunable bandgaps from 0.7 to 2.1 eV, exhibiting strong absorption for both visible and near-infrared (NIR) light.[59–62] Moreover, PbX QDs possess a large Bohr exciton radius, enabling efficient and balanced charge transport, particularly suitable for PV applications.[43,62]

To date, PVKs have achieved significant success in thin-film solar cells with a record PCE of ≈25%.[63–65] Their excellent photovoltaic properties, including large light absorption coefficient, tunable energy levels, long diffusion length for charge carrier, and low exciton binding energy, have attracted immense interest in QDs synthesis and technical applications.[66–69] PVKs have cubic crystal structures with a general formula ABX_3 (Figure 1d,e), where A represents a monovalent cation, B is a bivalent metal cation, and X stands for halides. Their QDs usually exhibit stable cubic structure relative to bulk perovskite. Similar to PbX QDs, PVK QDs feature size-dependent optoelectronic properties due to the quantum confinement effect. For instance, the absorption spectra edge of Cesium lead iodides ($CsPbI_3$) QDs can be tuned from 580 to 680 nm by varying the quantum dot size from 3.4 to 12.5 nm.[70] Furthermore, PVK QDs exhibit more defect tolerance than their PbX counterparts.[71–73] The high surface-to-volume ratio of QDs generally induces high defect states, but recent research found that those defect states do not act as traps in PVK QDs, thus contributing to a low photovoltage loss in PVK QD solar cells.[71,74–76] Since the first report in 2016, the PCE of PVK QD solar cells has soon overpassed their PbX counterparts and reached a certified record of 16.6% in 2020.[46,77]

It is not a coincidence that dominant materials in QD solar cells contain heavy metal Pb.[80,81] **Figure 2** depicts the band structures and atomic site-projected density of state (DOS) of PbS and formamidine lead iodides ($FAPbI_3$) bulk materials as examples. Pb-related orbitals play an important role and dominate conduction band (CB) edges for both material types. The $6s^2$ orbitals in stable Pb^{2+} ions not only empower direct bandgap transitions, bring strong antibonding coupling against the I^- 5p orbitals, but also provide a suitable dimension for asymmetric crystal structures.[82,83] Moreover, 6p orbitals compose the CB with a high DOSs, thereby resulting in strong photon absorption.[84] These properties render Pb-based semiconducting materials with great light-harvesting capability.

Figure 3 compares photovoltaic parameters of reported high-performance PbX and PVK QD solar cells, including open-circuit voltage (V_{oc}), short-circuit current density (J_{sc}), and fill factor (FF). As a general trend, PVK QD solar cells usually show higher V_{oc} and FF values but lower J_{sc} values than PbX QD solar cells. Concerning the SQ limit, both types of devices still have significant room to improve. So far, several reviews

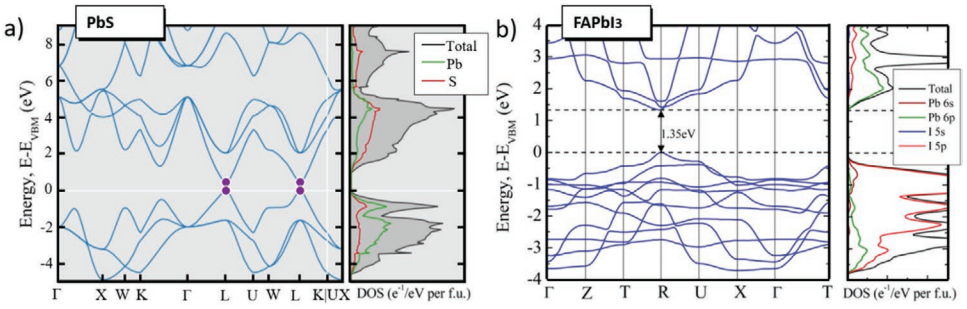

Figure 2. Band structures and atomic site-projected density of state (DOS) of a) PbS bulk materials, Reproduced under the terms of the CC BY licence.[78] Copyright 2015, The authors. and b) $FAPbI_3$ bulk materials. Reproduced with permission.[79] Copyright 2017, American Chemical Society.

© 2021 Wiley-VCH GmbH

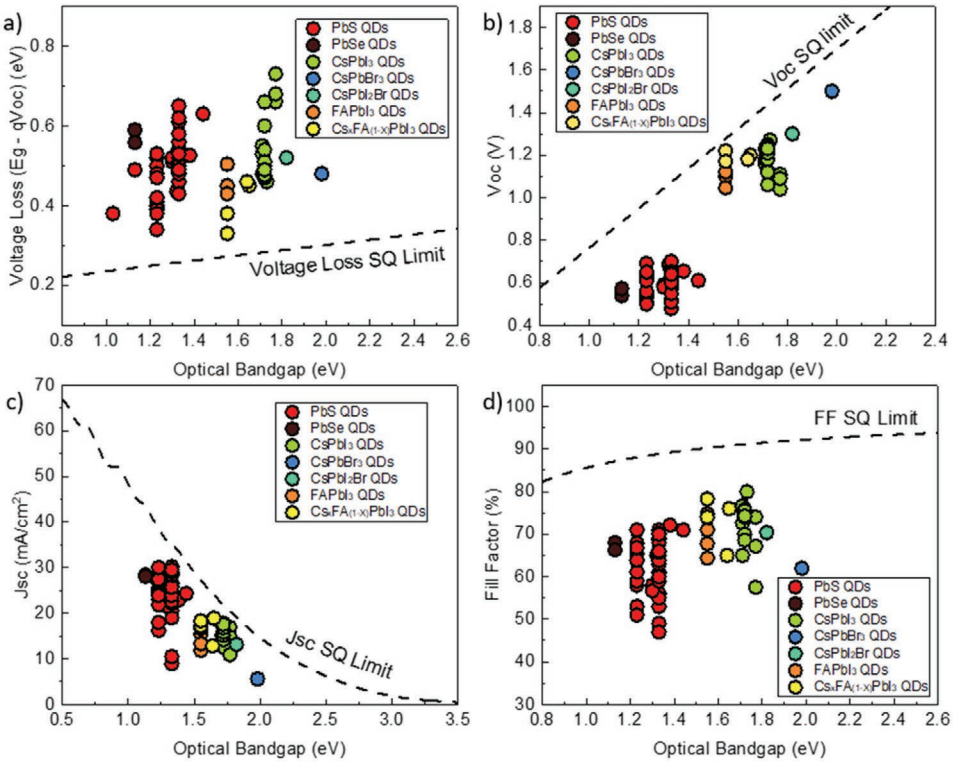

Figure 3. Comparison of photovoltaic parameters including a) voltage loss (E_g–qV_{oc}), b) open-circuit voltage (V_{oc}), c) short-circuit current density (J_{sc}), and d) fill factor (FF) versus device optical bandgap for reported high-performance PbX and PVK QD solar cells. Figures are drawn based on the data from Table 1.

were devoted to either PbX or PVK QD solar cells,[9–11,43,44,85–89] but no comprehensive comparison of these two emerging technologies. A comparison would enhance our understanding of QD solar cells and further realize their potentials. For instance, some well-developed performance-improving strategies for PbX QD solar cells may be applied as well to PVK QD solar cells. Judicious integration of these two types of QDs can also be an efficient route to further improve photovoltaic performance.[90]

In this review, we present an overview of state-of-the-art PbX and PVK QD solar cells, with a focus on their similarities and differences in terms of fundamental photophysics, device structures, and photovoltaic performance. First, an in-depth understanding of basic properties is discussed to compare PbX and PVK QDs from perspectives of quantum confinement effects, bandgap tuning, defect tolerance, and MEG. Then, breakthrough photovoltaic devices based on these two types of QDs are summarized side by side and comparatively reviewed from both device engineering and stability aspects. Finally, challenges for QD solar cells are presented along with an outlook for future technology developments.

2. Quantum Dot Physics

2.1. Quantum Confinement Effects

The unique quantum confinement effect of QDs has brought much research into the field. When confining the material size to nanoscale, the material's continuous energy spectrum will become discrete with an increased energy gap.[91–93] In general, to achieve the quantum confinement effect, the material's size needs to be reduced to a level that is comparable with its Bohr excitonic radius. By adjusting the size of QDs, the optoelectronic properties of the materials can be tuned.[28,94] According to the theory from Schmitt-Rink and coworkers, the ratio between the particle size and its Bohr radius plays an indispensable role in controlling quantum confinement.[95] A greater enhancement in nonlinear optical resonance and a larger tuning range are expected for smaller QDs. In other words, strong quantum confinement usually occurs to QDs with small sizes and large Bohr radii.[62]

For the PbX QD, its smaller electron and hole masses enable larger energy confinement. The Bohr radii of PbS and PbSe materials are 20 and 46 nm, respectively.[62] To date, a very small ratio (0.04) of the size-to-Bohr radius has been achieved for PbX QDs, while the energy gap can be tuned several times higher than corresponding bulk materials.[96,97] In contrast, due to the intrinsic low exciton binding energy, PVK materials usually have small Bohr radii (e.g., up to 12 nm for Cesium lead bromides ($CsPbBr_3$) QDs). Thus, it is difficult to obtain intense quantum confinement for PVK QDs.[70,98] For example, $CsPbBr_3$ QDs and their bulk counterparts show a negligible difference in the optoelectronic property as the QD size increases over 7 nm.[99]

2.2. Band Tuning

The energy bandgap is a critical parameter for semiconducting materials, especially for photovoltaic applications. Herein, both

© 2021 Wiley-VCH GmbH

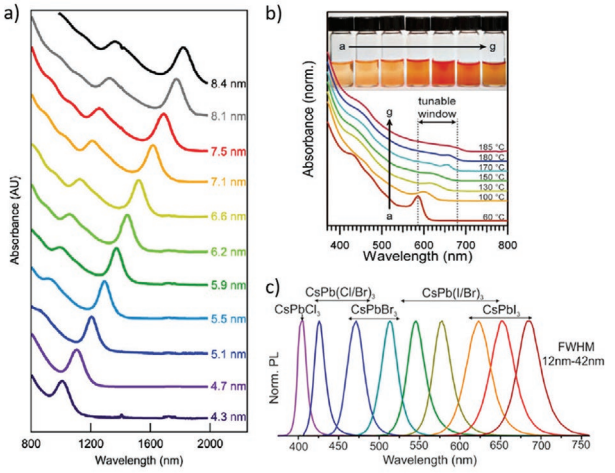

Figure 4. a) Bandgap tuning of PbS QDs over the spectrum from 800 to 2000 nm by varying the quantum dot size from 4.3 to 8.4 nm. Reproduced with permission.[29] Copyright 2014, American Chemical Society. b) Bandgap tuning of $CsPbI_3$ QDs over the spectrum from 580 to 680 nm by varying the quantum dot size from 3.4 to 12.5 nm. Reproduced with permission.[70] Copyright 2016, American Association for the Advancement of Science. c) Bandgap tuning of $CsPbX_3$ over the spectrum from 350 to 750 nm by compositional engineering with anion exchange method. Reproduced with permission.[98] Copyright 2015, American Chemical Society.

PbX and PVK QDs exhibit extraordinary bandgap-tuning abilities that are superior to other semiconducting materials.

Owing to robust quantum confinement, the bandgap of PbX QDs can be tuned across a very broad range by simple size modulation.[100,101] For instance, the absorption edge of PbS QDs was adjusted from the visible to the mid-infrared region by a size increase from 4.3 to 8.4 nm (**Figure 4**a).[29] Such a large bandgap tuning capacity enables facile energy level matching in solar cells, making PbX QDs promising candidates for tandem or multi-junction photovoltaic cell applications. Moreover, compositional engineering of PbX QDs with ternary alloys, such as PbS_xSe_{1-x}, further enlarges bandgap tuning capacity.[102,103] Ma and coworkers found that PbS_xSe_{1-x} QDs possess both advantages of PbS and PbSe QDs, and deliver better photovoltaic performance in solar cells.[104] In comparison, the bandgap tuning of PVK QDs is quite different. Suffering from weak quantum confinement, adjusting the QD size to realize broad range bandgap tuning is challenging for PVK QDs.[105,106] A significant increase in the $CsPbI_3$ QD size from 3.4 to 12.5 nm only resulted in a slight shift of the absorption edge from 580 to 680 nm (Figure 4b).[70] Generally, the broad-range bandgap tuning for PVK QDs relies on the compositional engineering of PVK materials.[86,107] Unlike simple PbX compounds, PVKs with the formula ABX_3 show diverse compositions. For PVK QDs, monovalent organic or metal ions, such as FA^+ and cesium (Cs^+), are commonly used as A-site cations, and divalent lead ions (Pb^{2+}) are utilized as the B-site cation. Halide elements, such as iodide (I), chloride (Cl), and bromide (Br), usually occupy the X anion position. As the valence band (VB) of PVK is dominated by halide orbitals from X-site halide anions, the bandgap tuning of PVK QDs can be realized by adjusting halide compositions.[108–110] The absorption edge of $CsPbX_3$ QDs can be tuned from 350 to 750 nm by engineering the composition of halide anions (Figure 4c).[98] Furthermore, the composition of A- and B-site cations can also be adjusted to further enlarge the bandgap tuning capacity of PVK QDs.[111–113]

Besides bandgap tuning, QDs show advantages in controlling band shift. Both the CB and VB of QDs can be intentionally modified by surface modification. It has been extensively reported that the energy level of PbX QDs can be substantially shifted. By switching surface ligands, the CB and VB of PbS QDs were varied with a maximum range of 0.9 eV.[29,94] Such controllable band shifting enables flexible energy level matching of PbS QDs in solar cells. Also, two types of PbX QDs with different ligand treatments were integrated for better band-alignment in quantum junction solar cells.[114] However, for PVK QDs, the development of such controllable band shifting is still very much in its infancy.[115] This may be due to inherent surface differences between PVK and PbX QDs.[10] Compared to PbX QDs, PVK QDs has a more ionic surface.[68] The ionic chemical bonding of PVK QDs makes them more sensitive to polar solvents. Therefore, well-established surface chemistry for band shifting in PbX QDs may not be effective for PVK QDs. Thus, exploring new surface chemistry strategies compatible with PVK QDs is highly demanded.

2.3. Defect Tolerance

Ascribed to the intrinsic high surface area, QDs are usually prone to various types of surface defects.[10,116–118] For instance, CdSe QDs suffer from the non-bonding localized orbitals resulting from the vacancy of Cd^{2+} ions. These orbitals are typical surface defects that cause mid-bandgap trap states, then induce non-radiative recombination in QDs.[10,117,119] Mid-bandgap trap states and low defect tolerance are critical issues for PbX QDs.[120,121] Although a large variety of surface chemistry treatments such as ligands exchanges have been developed to improve the optoelectronic properties of PbX QDs, these approaches may also produce suspended bonds, thus causing high defect density on its surface.[122–124] Consequently, PbX QDs usually suffer from relatively high voltage loss and need high-quality surface passivation when applied in solar cells.[125–127] Conversely, PVK QDs show a distinctly high defect tolerance. The electronic specificity of PVK QDs exhibits a high resistivity to material and surface defects.[75,86] In PVK QDs, referring to the formation energy, cation vacancies are dominant defects, while the ions in PVK QDs are difficult to be substituted. Such characteristic of PVK QDs makes it difficult to form anti-position defects in the mid-bandgap.[128] In general, for PVK QDs, most trap states are formed in the CB and VB rather than within the bandgap, which is the main cause that leads to its high defect tolerance.[72,73] Moreover, benefiting from the soft and dynamic crystal lattice, some electrons and holes can couple to form polarons in PVK QDs. These polarons can act as a shield to protect the exciton from trapping and scattering by defects, thus further increasing the defect tolerance.[129] Recently, Brinck and coworkers found that even a large number of ligand exchanges on the surface did not significantly increase the defect density, thus avoiding negative effects for $CsPbX_3$ QDs.[73] Overall, PVK QDs show an advantage over PbX QDs for their higher defect tolerance.

© 2021 Wiley-VCH GmbH

2.4. Multiple Exciton Generation

Besides the above-mentioned QD physics, MEG is another promising feature of QDs. For single-junction solar cells, the assumption that the absorbed photon can only activate one pair of the electron and hole from light excitation leads to the SQ limit for solar power conversion.[130] MEG of QDs, which produces two or more electron-hole pairs from one absorbed high-energy photon, offers the possibility to break the SQ limit and achieve higher PCE than other solar cells.[131,132] In QDs, an excited "hot" electron with an energy more than twofold of the bandgap can potentially benefit MEG.[133] When the "hot" electron relaxes from high-energy states, it has the chance to excite another electron from ground states, creating additional electron-hole pairs, rather than losing energy as the heat. This is because the relaxation of hot electrons is delayed in QDs and the extra energy in the excitonic transition process can be utilized in the presence of the quantum confinement effect.[134,135] It has been extensively reported that the MEG effect of QDs is strongly related to the ratio between the incident photon energy and the bandgap.[136,137] The threshold of MEG is usually considered at least twofold of the material bandgap.[133,135] For PbX QDs, many studies have demonstrated a pronounced MEG effect. For example, Semonin and coworkers reported the MEG effect with over 114% external quantum efficiency (EQE) and 130% internal quantum efficiency (IQE) for PbSe QD solar cells under excitation with threefold energy of the PbSe bandgap.[138] Davis and coworkers demonstrated a 122% EQE and a 150% IQE for solar cells comprising PbSe QD nanorods.[36] For PVK QDs, due to the larger bandgap of the PVK material, such an obvious MEG effect is harder to observe. Unlike PbX QDs showing narrow bandgaps, PVK QDs usually exhibit the bandgap over 1.7 eV, thus requiring a much higher MEG threshold.[66,139] Recently, Weerd and coworkers demonstrated that $CsPbI_3$ QDs showed the MEG effect with 98% quantum yield when the threshold excitation energy is higher than twofold of its bandgap.[140] Nevertheless, to date, no study has reported an obvious MEG effect with the EQE or quantum yield over 100% for PVK QDs. From this perspective, PbX QDs offer more substantial potential over PVK QDs for their lower MEG thresholds.

3. Engineering of Quantum Dot Photovoltaic Devices

3.1. Surface Chemistry

When applying QDs for solar cells, surface chemistry plays a vital role in determining its device performance. Long-chain organic ligands were normally employed during solution-phase synthesis to provide control over the size, crystallinity, and dispersion of QDs.[141,142] Besides, through ligand binding to the QD surface, these surface ligands can electronically passivate the QD to deliver desired optoelectrical properties as well as improved colloidal stability.[143,144] In specific, organic long-chain ligands (e.g., oleic acid, OA, and oleylamine, OLA) were widely adopted to impart QDs with desired mono-disperse and stability.[145] However, these insulating organic ligands hinder charge-carrier transport from dot-to-dot. In QD solar cells, QD surface chemistry serves a crucial role in both free carrier transport and QD film stability.[146] Abundant previous researches have revealed that using shorter conductive ligand for ligand substitution via ligand exchange processes can significantly improve the performance of the relevant QD solar cells.[147,148] It should be noted that the removal of the long insulating ligands on the surface of QDs can create surface defects, phase transition, and degradation of the QD, where re-passivation of the QD surface is then needed.[149] During the past decade, considerable reports of ligand-exchange have greatly improved the efficiency of PbX QD solar cells.[43,150] However, PbX and PVK QDs vary in size, shape, composition, and coordination of atoms within the crystalline structure. These variances result in the distinct QD surface environment, including ligand type, density, binding strength, etc.[10,86] Therefore, it is urgent to compare the QD surface conditions as well as their impact on the photovoltaic performance of PbX and PVK QDs.

To prepare conductive QD films, layer-by-layer (LBL) processes are normally carried out, in which QDs deposition and ligand exchanges (with short ligands) were repeated to yield desired film thickness for optimizing the device performance. In 2008, Sargent and coworkers first utilized a solid-state ligand exchange (SSLE) strategy for fabricating PbS QD solar cells.[151] In 2016, Luther and coworkers reported that methyl acetate (MeOAc), which is a partly polar solvent, enabled the removal of the insulating long ligands attached to $CsPbI_3$ PVK QD surface and led to the first PVK QD solar cell with PCE over 10%.[70] Unfortunately, after removing the surface organic long passivating ligands, surface traps appear due to the formation of vacancies and surface dangling bonds. These nefarious surface traps need to be re-passivated using conductive ligands for improving carrier transport between neighboring QDs.[149]

In the context of PbX QD solar cells, as shown in **Figure 5**a, early researchers employed shorter functional ligands such as organic thiols (benzenedithiol (BDT), ethanedithiol (EDT)), amines (ethylenediamine (EDA), tetrabutylammonium iodide (TBAI)), bi-functional 3-mercaptopropionic acid (MPA) for SSLE and passivation.[43,44] In these cases, the inter-dot distance was significantly reduced from ≈2 nm for OA-PbS QD solids to less than <0.5 nm in the case of EDA-PbS. Decreased inter-dot distance can cause an enhancement in the electronic coupling between QDs and make charge transport more efficient, as further confirmed by the photovoltaic performance.[152,153] Later, the introduction of inorganic halides such as Br and I atoms, and Pb salts such as PbI_2 and $PbBr_2$ was demonstrated. Inorganic halides have an enhanced passivation effect on the trap site, which the large molecular MPA cannot access, thereby enhancing the device performance.[154,155] As shown in Figure 5b, for OA/OLA-capped $CsPbX_3$ QDs, using a moderate polar solvent like MeOAc is a standard protocol to fabricate conductive QDs solid films for photovoltaic applications.[70] Compared to PbX QDs, the chemical bonding in PVK QDs is more ionic and the QD surface is more sensitive to polar solvents.[68] MeOAc was first reported to exchange native oleate ligands with short acetate molecules in the presence of moisture.[156] Cation halide salts (e.g., FAI) were usually used as an additional treatment in the preparation of $CsPbI_3$ QD solid films and exchange residual

© 2021 Wiley-VCH GmbH

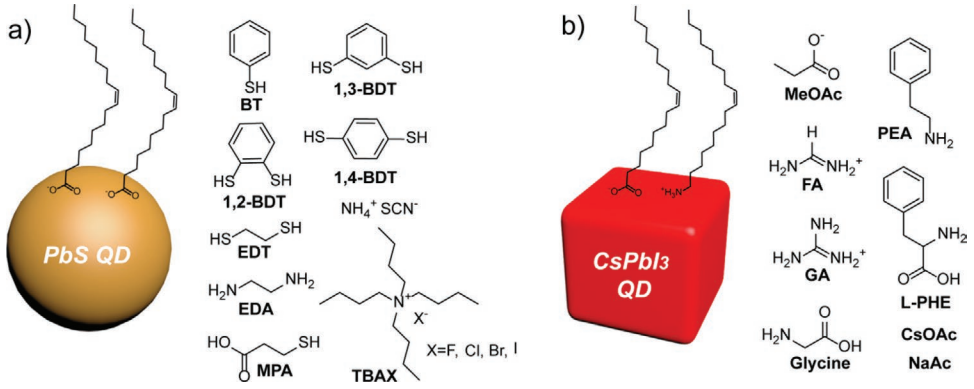

Figure 5. Initial and post-passivating ligands in a) PbS and b) $CsPbI_3$ QDs.

oleylammonium$^+$.[157] However, MeOAc has a slow hydrolysis nature if it is not processed with acids and bases, and as a result the removal of oleate ligands is less efficient.[145] Down this line of research, lots of organic (e.g., secondary amine, thiols, guanidinium salts, and zwitterion ligands) and inorganic (cesium and sodium salts) short ligands were dissolved in MeOAc or used to replace organic ligands.[87,144–146,158–161] In comparison with PbX QDs, surface ligand exchange of PVK QDs is far behind from perspectives of ligands diversity and sophistication. It is of great necessity to develop a more efficient approach for the removal of native ligands in PVK QD solar cells, which is expected to further enhance the carrier transport and device performance.

Regarding the QD film fabrication, the LBL process involving SSLE is both time- and material-consuming, and incompatible with the industrial scale-up printing technique. Alternatively, ligand exchange can be processed in a solution phase. The solution-phase ligand exchange (SPLE) can be performed using customized QD inks to directly form conductive solids in a single step with controllable film thickness, which opens a new avenue for large-scale QD PV fabrication.[162,163] Talapin and coworkers first realized SPLE in the CdSe QD solution using inorganic molecular metal chalcogenides for applications in high-performance field-effect transistors.[164] Sargent and coworkers used *n*-butylamine to exchange the OA of PbS in the solution phase and demonstrated relevant applications in solar cells.[165] In the early development stage, the photovoltaic performance based on these inks lagged behind those based on SSLE, which is attributed to the increased surface traps. Inspiring by the metal-halide hybrid perovskites, halometallate, halide, and pseudo-halide contained PbS QD inks were reported with significantly improved optical properties, surface passivation and carrier mobility.[166] In 2014, Sargent and coworkers employed SPLE-processed QDs capped with iodide ligands for fabricating solar cells with a PCE of ≈6%, which is comparable with devices produced from LBL SSLE.[167] In 2017, the same group demonstrated SPLE PbS QD solar cells with PbX_2/NH_4Ac ligands achieving a certified record PCE of 11.28%.[168] They reported that solution-phase ligand exchanged QD inks can enable a flat energy landscape and higher QDs packing density. The addition of NH_4Ac in hybrid QD inks can assist the colloidal stabilization, maximize the amount of halides on QD surfaces, and make the removal of organic long-chain ligands more efficient. Additionally, the pre-exchanged PbS QD ink significantly simplifies the fabrication of QD solar cells and exhibits superior efficiency and stability relative to the SSLE based one. These improvements provide a new protocol for high-performance PbS QD solar cells and open a new not been reported avenue for the future development of QD solar cells. In contrast, SPLE in PVK QDs has rarely been explored yet. It has been recognized that PbS QDs and PVK QDs vary significantly in the coordination of atoms in their crystalline structures. As a result, the SPLE method is widely used in PbS QD solar cells but cannot be directly transferred to prepare scalable PVK QD inks. In 2016, Manna and coworkers fabricated scalable and environmentally friendly PVK inks, which consisted of $CsPbBr_3$ QDs as a colloidal suspension with shorter ligands, demonstrating the possibility of SPLE in PVK QDs.[77] So far, solid-state processes are still the dominant ligand exchange methods for PVK QDs,[10] while the SPLE process is highlighted herein, which may push forward the future PV performance of PVK QDs.

3.2. Device Structure Engineering

The PCE of PbX QD solar cells has been boosted to over 13% in the past decades. Besides the progress of QD surface chemistry, optimizing device structure is an effective strategy to improve PV performance. In general, the development of device architecture can be divided into three different stages (**Figure 6**a). Before 2010, inspired by traditional inorganic solar cells, the simple Schottky junction structure (QD absorber layer sandwiched between the top metal and bottom indium tin oxide (ITO) electrode) was dominant in PbX QD solar cells.[169,170] Unfortunately, there are two main issues limiting the enhancement of PV efficiency. One is the relatively low charge collection efficiency (small minority carrier diffusion lengths), the other is limited V_{oc} as a consequence of Fermi-level pinning. Therefore, the efficiency improvements of such Schottky architecture mainly rely on efforts in optimizing QD compositions and surface chemistry, and the highest reported PCE of 5.2% was obtained based on PbS QDs.[171]

In the second stage, in order to improve the charge collection efficiency, a depleted heterojunction (DHJ) structure, which incorporated n-type metal oxides (Titanium dioxide

© 2021 Wiley-VCH GmbH

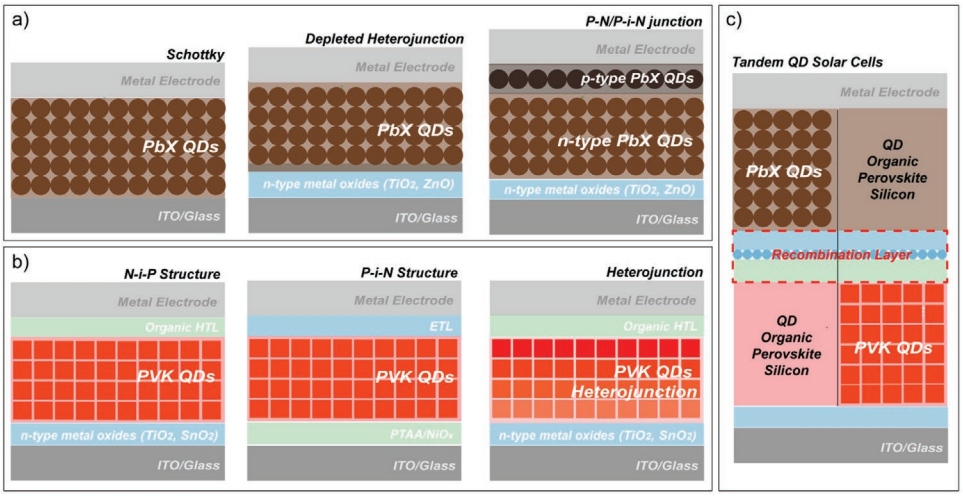

Figure 6. a) Schottky, DHJ, and P-N/P-i-N quantum junction device architecture of PbX QD solar cells. b) N-i-P, P-i-N, and heterojunction device architecture of PVK QD solar cells. c) Device architecture of tandem solar cells based on PbX or PVK QDs.

(TiO_2), zinc oxide (ZnO), or zinc magnesium oxide (ZnMgO)) inserted between p-type PbX QDs and bottom ITO electrode, was adopted by the community.[172,173] Although the DHJ architecture overcame the bottleneck of the charge extraction from the Schottky structure and enhanced PV performance, the excitons generated at the position close to the metal electrode in the device were extracted via diffusion. In DHJ PV design, QD surface passivation as well as tuning the morphology of n-type metal oxide layers (such as porous, nano-pillar, nanowire of TiO_2, or ZnO) allow efficient charge dissociation and enable the application of thicker active films which can absorb more light.[174,175] These concepts finally led to the improved PCE of DHJ PbS QD solar cells over 9%.[176]

For the last stage, Sargent and coworkers first reported quantum homojunction architecture utilizing n- and p-type PbS QD layers for enhanced light harvesting in 2012.[177] After extensive optimization of the surface ligands, Bawendi and coworkers reported the use of mildly n-type TBAI-PbS QDs stacked with a thin p-type EDT-PbS QD layer as an active layer.[94] They used ZnO as an electron transporting layer, and such an optimized N-i-P architecture integrates DHJ with P-N quantum homojunction. This device structure exhibits advantages of high reproducibility and air stability together with a certified PCE of 8.55%, which created new pathways for PbS QD PVs. Further QD surface and device interface optimization as well as the incorporation of hole transport layer (HTL) first produced PbS QD PV with over 10% efficiency, which is widely recognized as an efficiency threshold for commercializing new generation solar cells.[178] As mentioned, SPLE PbS QDs can be used for single-step deposition of QD films, which was adopted to replace the TBAI-PbS QD layer fabricated from LBL, obtaining a record efficiency approaching 12% for PbS QD solar cells.[179]

It is worth noting that p-type EDT-PbS QD is dominant in an N-i-P configuration since the EDT-PbS QD layer can be processed in ambient conditions forming good Ohmic contact and energy alignment with the QD active layer and Au electrode.[29,94] However, the deposition of the EDT-PbS QD layer still relies on the solid-state ligand-exchange process and the LBL method, which is not ideal for scalable fabrication of solar cells.[180] It was recognized that developing pre-exchanged QD inks for HTL is an effective method to solve the problem. Jang and coworkers used the sulfur-exchanged p-type QD inks to fabricate the HTL in QD solar cells and demonstrated a comparable device performance with the device based on SSE processed HTL.[181] Moreover, exploring alternative one-step processed organic HTL is of significance to further improve the scalability of PbX QD devices. Continuous efforts in organic functional conjugated polymer design and fabrication rapidly improve the PCE of PbS N-i-P QD solar cells from below 9% to now over 13%, demonstrating the potential of both organic HTL and N-i-P quantum junction configuration.[180,182,183] Recently, Jang and coworkers designed a type of organic π-conjugated polymer, PBDTTPD-HT, as HTL for QD solar cells and proved a device PCE of 11.53%.[184] Park and coworkers developed a new random polymeric HTL, asy-ran PBTBDT, and fabricated PbS QD solar cells showing a PCE of 13.2%.[185]

In addition, there are a few other noteworthy device engineering strategies. Sargent and coworkers developed PbS QD solar cells with a bulk heterojunction device structure based on a homogeneous n-type and p-type QDs mixed film.[47] They introduced a cascade surface modification strategy for QDs, which made n-type and p-type PbS QDs become fully miscible in the same solvent. As a result, the carrier diffusion length of the QD bulk film was improved by 1.5 times, and the fabricated bulk heterojunction PbS QD solar cells exhibited a remarkable PCE of 13.3%. More recently, the same group applied monolayer perovskite bridges on PbS QDs and demonstrated a high PCE of 13.8% for their fabricated devices.[55] In this work, they deposited the perovskite layer after the fabrication of the QD solid rather than mixing perovskite and QD solution together. As a result, they proved that the perovskite monolayer can improve the interdot coupling in the QD film, thereby increasing the film mobility by 3 times.

In comparison, the development of the device structure of PVK QD solar cells followed a different route. Since the

© 2021 Wiley-VCH GmbH

first report in 2016 using fully inorganic $CsPbI_3$ PVK QD, the progress in PVK QD solar cells has rapidly improved with the latest PCE exceeding 16%.[46] A range of material improvements has occurred with fully inorganic $CsPbX_3$ QDs to organic-inorganic hybrid PVK QDs, such as $FAPbI_3$ and mixed-cation $Cs_{1-x}FA_xPbI_3$.[145] So far, as shown in Figure 6b, $CsPbI_3$ QDs have been applied mainly in "conventional" structured (N-i-P) devices coupled with n-type transition metal oxide (TiO_2 or Tin oxide (SnO_2)) and p-type organic HTLs (Spiro-OMeTAD, PTB7 or PTAA). Recently, to tackle with the stability issue, replacing Spiro-OMeTAD with other organic HTLs has become a hot research topic.[186] The Spiro-OMeTAD layer shows poor thermal stability and can have severe morphological deformation at high temperatures.[187] Pure Spiro-OMeTAD film usually has low hole mobility and conductivity, which make electronic doping unavoidable for its application as HTL in solar cells.[188,189] Commonly used dopants such as bis(trifluoromethane)sulfonamide lithium (Li-TFSI) and 4 *tert*-butyl pyridines (tBP) can increase the mobility of Spiro-OMeTAD, but they also exacerbate the hydrophilic nature of the film and thus cause instability in the device.[190] In comparison, other organic HTLs such as PTB7 and PTAA showing better stability are more promising alternatives.[191,192] Nevertheless, these organic HTL materials need purification and can be costly, hindering future industrialization of the N-i-P device.[44,87] P-i-N cells with bulk thin-film perovskites can achieve performance comparable to N-i-P ones and show advantages of better stability and tandem device compatibility.[193] Unfortunately, the $CsPbI_3$ QD solar cells with a P-i-N geometry (using PTAA as HTL) demonstrated poor photovoltaic performance with a low V_{oc}, where the poor QD film deposition onto PTAA is the culprit.[194] Quite recently, Halpert and coworkers demonstrated efficient P-i-N all-inorganic $CsPbI_3$ PVK QD solar cells with an improved PCE up to 13.1% enabled by the inorganic HTL NiO_x.[195] We believe the P-i-N structure will catalyze the development of more robust and cost-effective PVK QD solar cells.

Due to the ionic nature, the post-synthetic process for PVK QDs can be simpler than the PbS counterpart. The compositional engineering of PVK is achievable with the post-synthetic ion exchanges without changing the QD size and shape.[86] For example, a wide compositional range of $Cs_{1-x}FA_xPbI_3$ (x = 0–1) can be easily obtained through the cation exchange, which shows superiority over pure $CsPbI_3$ or $FAPbI_3$ QD solar cells. It is worth noting that the record PCE for QD solar cells of 16.6% was obtained with a $Cs_{0.5}FA_{0.5}PbI_3$ composition.[46] Engineering film processing and device structure is also effective to improve device performance. Luther and coworkers reported PVK QD PV devices based on a device structure of internal heterojunction (Figure 6b), which used two layers of PVK QD films as the absorber with a $CsPbI_3$ QD layer on top of a $Cs_{1-x}FA_xPbI_3$ QD layer.[196] The composition of such a heterojunction can be easily tuned by the spin-coating procedure with different layer thicknesses. This approach can produce PVK QD solar cells with over 16% efficiency. Meanwhile, the authors of this review fabricated a $CsPbI_3/FAPbI_3$ PVK QD bilayer in a similar device structure and demonstrated the PCE of 15.6%.[139] In addition, with the protection of upper $FAPbI_3$ perovskite QD films, the ambient stability of such PVK QD solar cells is significantly improved. Very recently, we introduced a hybrid layer consisting of PCBM and $CsPbI_3$ QDs between the SnO_2 electron transport layer and $CsPbI_3$ QDs for fabricating solar cells, which enabled a PCE of 15.1%.[18] Overall, PVK QDs provided a facile way to fabricate multiple layers and quantum junctions for optoelectronic applications.

Furthermore, both PbX and PVK QDs can be utilized for fabricating tandem solar cells. The tandem solar cell, which connects sub-cells with different bandgaps, is an effective approach to minimize energy losses and fully utilize solar spectrum relative to single-junction solar cells.[197] In this regard, tandem solar cells were considered as an ideal platform to marry the conventional PbX QDs and the recently developed PVK QDs. Among all the solution-processed photovoltaic materials, PbX QDs have one of the widest bandgap tuning range of 0.7–2.1 eV, which can provide the tandem device with strong NIR absorption.[59–62] In tandem solar cells based on PbX QDs, synthesizing QDs with different sizes for the front and the bottom cell can help the device achieve complementary absorption.[198,199] Besides, PbX QDs can act as ideal rear cells connecting with wide-bandgap organic photovoltaic, thin-film PVK, or even silicon solar cells in a tandem configuration (Figure 6c).[200] Indeed, combination of 1.55 eV PVK QDs and 1.0 eV PbS QDs in tandem solar cells is predicted to show a theoretical PCE of 43%.[201] However, so far, only a few tandem devices based on PbX QDs/QDs, organic/PbX QDs, perovskite/PbX QDs, and Si/PbX QDs have been successfully demonstrated, which is due to the lack of an efficient solution-processed recombination layer to connect the sub-cells.[199,201–203] Ma and coworkers reported the all-QD tandem device by using PbS QD solar cells as both front and bottom sub-cells.[204] Their fabricated devices exhibited a high PCE approaching 9% which is 2 times higher than the corresponding single-junction device. Recently, Sargent and coworkers combined PbS QD solar cells with OSCs to fabricate organic/QD hybrid tandem devices,[205] and they demonstrated a high PCE of 13.7% for their fabricated devices with a dual NIR absorber.

In contrast, the bandgap of the current most efficient PVK QDs ($CsPbI_3$) is 1.73 eV, which is the ideal bandgap for the application as front cells in tandem devices, especially for Si tandem solar cells (Figure 6c).[206] As discussed in the previous section, post-synthesis ion exchanges have been utilized to flexibly tune the $CsPbX_3$ QDs absorption from 500 to 730 nm, which also enables a flexible bandgap match between the front cell and the bottom cell.[98] However, due to the short history of $CsPbX_3$ QD PV, there has been no report of tandem devices using these emerging PVK QDs, which will surely become an active and promising research direction in the near future. In general, QD films are fabricated with mild solvents, where the deposited QD film is insoluble in most organic solvents. Such a feature also ensures the high processability of QD films to be applied in multi-junction devices.[10] The use of QDs in tandem cells can enhance the compatibility with various materials, and also reduce the cost. The device structures and PV performance of representative PbX and PVK QD solar cells over the past decade are summarized in **Table 1**.

© 2021 Wiley-VCH GmbH

Table 1. Photovoltaic parameters of some representative QD solar cells.

Year	Device structure	E_g [eV]	V_{oc} [V]	J_{sc} [mA cm^{-2}]	FF	PCE	Ref.
PbX QD							
2010	ITO/ZnO/PbS/Au	1.33	0.588	8.9	55.97%	2.94%	[207]
2010	SnO2:F/TiO_2/PbS/Au	1.33	0.51	10.5	60.00%	3.40%	[208]
2010	SnO2:F/TiO_2/PbS/Au	1.23	0.51	16.2	58.00%	5.10%	[172]
2011	FTO/TiO_2/PbS/Au	1.33	0.48	20.6	56.00%	5.50%	[209]
2011	FTO/TiO_2/PbS-TBAI/Au/Ag	1.23	0.53	18.0	59.00%	5.54%	[210]
2012	FTO/TiO_2/ZnO/PbS/MoO_x/Au/Ag	1.30	0.59	21.8	58.00%	7.40%	[153]
2012	FTO/TiO_2 /PbS/MoO_x/Au/Ag	1.33	0.57	19.0	49.00%	5.60%	[211]
2012	ITO/p-PbS/n-PbS/Al/Ag	1.33	0.52	22.2	47.00%	5.40%	[177]
2013	FTO/TiO_2/PbS/MoO_x/Au/Ag	1.33	0.61	22.5	53.00%	7.30%	[212]
2013	ITO/p+-PbS/n-PbS/n+-PbS/AZO/Ag	1.33	0.55	24.5	55.00%	7.40%	[114]
2013	FTO/TiO_2/PbS/MoO_3/Au/Ag	1.33	0.62	22.7	61.00%	8.50%	[213]
2013	ITO/ZnO/PbS-TBAI/PbS-EDT/MoO_x/Al	1.33	0.55	24.2	63.80%	8.55%	[94]
2014	FTO/TiO_2/PbS/MoO_3/Au/Ag	1.30	0.58	21.5	56.70%	7.07%	[214]
2014	FTO/TiO_2/PbS-I/PbS-MPA/MoO_3/Au/Ag	1.23	0.50	23.0	53.00%	6.10%	[167]
2014	FTO/TiO_2/n+-PbS/p-PbS/p+-PbS/MoO3/Au/Ag	1.33	0.51	26.6	59.00%	8.00%	[155]
2015	ITO/TiO_2/PbS-PbI_2/PbS-MPA/MoO_x/Al	1.23	0.56	25.5	51.00%	7.30%	[215]
2015	ITO/ZnO/PbS-$MAPbI_3$/PbS-EDT/Au	1.23	0.61	21.8	67.90%	8.95%	[216]
2016	FTO/TiO_2/PbS-TBAI/PbS-EDT/MoO_3/Au	1.33	0.61	25.8	60.00%	9.40%	[217]
2016	ITO/ZnO/PbS/MoO_x/Ag	1.33	0.55	24.8	66.00%	9.01%	[218]
2016	ITO/ZnO/PbS/Au	1.33	0.67	22.2	69.00%	10.26%	[219]
2016	ITO/ZnO/PbS-I/PbS-EDT/MoO_3/Au/Ag	1.33	0.63	23.5	65.00%	9.60%	[127]
2016	ITO/ZnO/PbS-TBAI/PbS-EDT/GD/Al	1.38	0.65	22.8	72.14%	10.64%	[178]
2016	ITO/ZnO/PbS-MAI-TBAI/PbS-EDT/Au	1.44	0.61	24.3	71.00%	10.60%	[220]
2017	ITO/ZnO-JTCA/PbS-PDMII/PbS-PDT/Au	1.32	0.68	24.6	65.00%	10.83%	[221]
2017	ITO/ZnO-Cl/PbS/Au	1.23	0.63	28.5	65.36%	11.63%	[222]
2017	ITO/ZnO/PbS-AA-TBAA/PbS-EDT/Au	1.23	0.69	24.8	61.10%	10.50%	[223]
2017	ITO/ZnO/PbS-EMII/PbS-EDT/Au	1.33	0.65	22.6	71.00%	10.47%	[224]
2017	ITO/ZnO/PbS-TG:PbS-$MAPbI_3$/PbS-EDT/Au	1.23	0.62	26.8	63.90%	10.45%	[225]
2017	ITO/MZO/PbS-TBAI/PbS-EDT/Au	1.33	0.62	24.7	68.00%	10.40%	[226]
2018	ITO/ZnO/n-PbS/p-PbS/Au	1.23	0.64	23.9	71.00%	10.91%	[181]
2018	ITO/ZnO-EAL/PbS-I/PbS-PDT/Au	1.33	0.67	23.9	68.00%	10.75%	[227]
2018	ITO/ZnO/PbS-I/PbS-MPA/p-MeO-TPD/Ag	1.33	0.70	25.7	65.03%	11.71%	[228]
2018	ITO/ZnMgO/PbS-PbI_2/Ag-PbS-EDT/Au	1.33	0.63	25.9	63.00%	10.30%	[229]
2018	ITO/ZnO/PbS-I/PbS-I/PbS-EDT/Au	1.33	0.63	28.8	68.00%	12.30%	[230]
2018	ITO/ZnO/PbS-TBAI/PbS-EDT/Au	1.33	0.63	25.8	68.80%	11.21%	[179]
2018	ITO/ZnO/PbS-PbI_2/PbS-EDT/Au	1.33	0.65	29.0	63.80%	12.01%	[165]
2019	ITO/SnO_2/PCBM/PbSe-PTLE/PbS-EDT/Au	1.33	0.54	28.4	68.00%	10.40%	[231]
2019	ITO/ZnO/PbS/PbS-EDT/Au	1.23	0.61	27.4	66.82%	11.18%	[163]
2019	ITO/ZnO/PbSe-PbI_2/PbS-EDT/Au	1.33	0.572	28.1	66.30%	10.68%	[232]
2019	ITO/ZnO/PbS/PBDB-T(F)/MoO_3/Ag	1.33	0.60	28.4	65.80%	11.20%	[180]
2020	ITO/ZnO/n-PbS:p-PbS/PbS-EDT/Au	1.33	0.65	30.2	68.00%	13.30%	[47]
2020	ITO/ZnO/PbS/PbS-MA/Au	1.33	0.64	29.1	70.00%	13.00%	[233]
2020	ITO/ZnO/PbS-$PbBr_2$/PbS-EDT/Au	1.33	0.64	29.5	66.00%	12.50%	[234]
2020	ITO/ZnO/PbS-FABr/PbS-EDT/Au	1.23	0.65	30.0	71.00%	13.80%	[55]

© 2021 Wiley-VCH GmbH

Table 1. Continued.

Year	Device structure	E_g [eV]	V_{oc} [V]	J_{sc} [mA cm^{-2}]	FF	PCE	Ref.
PVK QD							
2016	FTO/TiO_2/$CsPbBr_3$/Spiro-MeOTAD/Au	1.98	1.50	5.6	62.00%	5.40%	[77]
2016	FTO/TiO_2/$CsPbI_3$/Spiro-MeOTAD/MoO_x/Al	1.71	1.23	13.5	65.00%	10.77%	[70]
2017	FTO/TiO_2/$CsPbI_3$/Spiro-MeOTAD/MoO_x/Al	1.71	1.16	15.2	76.63%	13.58%	[68]
2018	FTO/TiO_2/μGR-$CsPbI_3$/PTAA/Au	1.71	1.18	13.6	72.60%	11.64%	[157]
2018	FTO/TiO_2/$CsPbI_3$/PTB7/MoO_x/Ag	1.73	1.27	12.4	80.00%	12.55%	[235]
2018	ITO/TiO_2/$CsPbI_2Br$/P3HT/Au	1.82	1.30	13.1	70.40%	12.02%	[236]
2018	ITO/SnO_2/$FAPbI_3$/Spiro-OMeTAD/Au	1.55	1.10	11.8	64.40%	8.38%	[237]
2019	FTO/TiO_2/$CsPbI_3$/Spiro-OMeTAD/Au	1.77	1.04	16.9	67.20%	11.87%	[143]
2019	FTO/TiO_2/$CsPbI_3$/Spiro-MeOTAD/MoO_x/Ag	1.72	1.18	15.2	74.20%	13.30%	[158]
2019	FTO/TiO_2/$CsPbI_3$/PTAA/MoO_x/Ag	1.72	1.25	15.0	75.60%	14.10%	[160]
2019	FTO/TiO_2/$CsPbI_3$/Spiro-OMeTAD/Au	1.77	1.11	14.8	74.00%	12.15%	[238]
2019	FTO/TiO_2/$CsPbI_3$:Yb/PTB7/MoO_x/Ag	1.72	1.25	14.2	74.00%	13.12%	[191]
2019	ITO/PTAA/$CsPbI_3$/C60/BCP/graphene	1.77	1.09	10.9	57.50%	6.80%	[206]
2019	ITO/PTAA/$CsPbI_3$/C60/BCP/Cu	1.72	1.12	17.1	70.00%	13.40%	[239]
2019	ITO/SnO_2/$FAPbI_3$/Spiro-OMeTAD/Ag	1.55	1.10	15.4	74.80%	12.70%	[240]
2019	FTO/TiO_2/$FAPbI_3$/Spiro-OMeTAD/Au	1.55	1.05	13.3	67.80%	9.42%	[241]
2019	ITO/TiO_2/$Cs_{0.25}FA_{0.75}PbI_3$/$CsPbI_3$/Spiro-OMeTAD/Al	1.65	1.20	18.9	76.00%	17.39%	[196]
2019	FTO/TiO_2/$(FA_{0.81}Cs_{0.19})Pb(I_{0.81}Br_{0.19})_3$ /Spiro-OMeTAD/MoO_x/Al	1.64	1.18	12.8	65.00%	9.86%	[242]
2019	FTO/TiO_2/$CsPbI_3$/$FAPbI_3$/PTAA/MoO_x/Ag	1.55	1.22	17.2	74.00%	15.60%	[139]
2020	FTO/TiO_2/$CsPbI_3$/Spiro-OMeTAD/Au	1.72	1.06	17.8	75.80%	14.32%	[243]
2020	ITO/SnO_2/$Cs_{0.5}FA_{0.5}PbI_3$/Spiro-OMeTAD/Au	1.55	1.17	18.3	78.30%	16.60%	[46]
2020	FTO/TiO_2/$CsPbI_3$/Spiro-OMeTAD/MoO_3/Ag	1.72	1.23	15.3	74.80%	14.10%	[244]
2020	FTO/TiO_2/$CsPbI_3$/PBDB-T/MoO_x/Ag	1.72	1.22	15.1	75.00%	13.80%	[145]
	FTO/TiO_2/$FAPbI_3$/PBDB-T/MoO_x/Ag	1.55	1.12	16.7	71.00%	13.20%	
2020	FTO/TiO_2/$CsPbI_3$/PTAA/MoO_x/Ag	1.72	1.24	15.8	75.50%	14.90%	[145]
2020	FTO/TiO_2/$CsPbI_3$/PbSe/Spiro-OMeTAD/Ag	1.72	1.21	16.8	68.60%	13.90%	[90]
2020	FTO/TiO_2/GASCN+TA-$CsPbI_3$/PTAA/MoO_x/Ag	1.72	1.25	15.9	76.70%	15.21%	[159]
2020	ITO/SnO_2/PCBM/$CsPbI_3$/PTB7/MoO_x/Ag	1.72	1.26	15.2	78.00%	15.10%	[18]
2020	FTO/TiO_2/$CsPbI_3$/Spiro-OMeTAD/MoO_x/Ag	1.72	1.23	17.6	74.30%	16.07%	[245]

4. Stability of Quantum Dot Photovoltaic Devices

4.1. Degradation Mechanisms

Besides PV performance, device stability is considered as another key factor dictating the potential industry-scale deployment of solar cells. Currently, the poor stability of QD solar cells is a bottleneck that hinders their applications and commercialization. The surface of QDs, enriched with defects such as dangling bonds, facets, and corner sites, can dynamically interact with certain environmental factors, which is one of the root reasons for the instability of QDs.[146] Since PbX QDs exhibit lower defect tolerance than PVK QDs, the degradation of PbX QDs is more sensitive to the surface changes than PVK QDs. The defects on the QD surfaces during the degradation can cause trap states for photo-generated excitons and ultimately deteriorate the device performance.[246] When PbS QDs are exposed to ambient air, the oxygen can react with the S atom, leading to the formation of lead sulfate ($PbSO_4$) and lead sulfite ($PbSO_3$) on the QD surface.[247,248] Compared to $PbSO_3$, the formation of $PbSO_4$ is more responsible for the degradation of PbS QDs since it will create mid-bandgap traps with a depth of around 0.3 eV below the CB.[249] Similarly, for PbSe QDs, oxidation products such as PbO, SeO_2, and $PbSeO_3$ can be formed on their surface in the presence of air.[250,251] Such air-induced degradation for PbSe QDs is even faster than PbS QDs since the Se atom is more chemically reactive than the S atom.[17] For PbX QDs, the QD surface has two types of facets with different crystal orientations, namely (100) and (111). The polar (111) facet is Pb-rich, while the non-polar (100) facet has a stoichiometric Pb to X ratio.[252,253] After interacting with surface ligands for charge balance, (111) facets show higher resistivity to oxidation than (100) facets, as most of the surface sites on (111) facets can be well-passivated.[254] Compared to (100) facets, (111) facets have a denser ligand shell hindering oxidant diffusion.[146] This explained why $PbSO_3$ is the main oxidation product for (111)

© 2021 Wiley-VCH GmbH

facets, while the formation of $PbSO_4$ dominants the oxidation of (100) facets in PbX QDs.[247] In most cases, (111) facets are more stable than (100) facets for PbX QDs. Indeed, smaller PbX QDs with higher (111)/(100) facets ratios usually exhibit better stability than larger PbX QDs.[255] In addition to the oxidation, some QD surface species can also cause the light instability of QD solar cells.[127] For example, the hydroxides can be attached to the QD surface after the ligand exchange for both PbS and PbSe QDs. These hydroxide sites can quench the excited electron-hole pairs, thereby aggravating the non-radiative recombination in QDs to deteriorate the device performance under illumination.[127,256]

PVK QDs also have instability issues induced by the dynamic QD surface, where surface capping ligands play an important role. Dynamic ligand exchanges, such as the exchange between OA and OAm, can cause agglomeration of PVK QDs and result in performance degradation of the device.[257] When exposed to high-temperature thermal stress, surface ligands of PVK QDs can be detached to create surface defects.[258] Therefore, ligands owning strong binding to PVK QDs are preferred, which can hinder the light-induced aggregation of PVK QDs and thus improve the light stability of the device.[259] In addition, PVK QDs are sensitive to polar solvents due to their ionic nature.[260] The polar solvent can dissociate surface atoms of QDs, which causes QD agglomeration and increase the surface defects. Afterward, moisture can penetrate through those surface defects to further destroy the PVK QDs and degrade the device performance.[261] Moreover, PVK QDs have a different structural and phase stability issue when compared to PbX QDs.[262,263] The optoelectronic properties of PVK materials are related to their crystal structures. Ideally, the PVK material has a 3D symmetric cubic crystal structure with the Goldschmidt tolerance factor (t) equals to 1. However, most of the PVK materials show a tolerance factor below 1 and exhibit rhombohedral or orthorhombic structures. Under this circumstance, crystal distortion and phase transition can occur to detrimentally affect the optoelectronic properties of PVK materials as well as the device performance of PVK QD solar cells.[262]

Depending on the composition, PVK materials show various degradation mechanisms under light, thermal, and air stresses.[264,265] For PVKs containing organic cations, degradation induced by moisture is considered as one of the most critical issues. Owing to the hygroscopic nature of amine salt, the PVK can react with the moisture to form hydrate products such as $(CH_3NH_3)_4PbI_6.2H_2O$.[266] Such a reaction breaks the hydrogen bond between the inorganic and organic units and then decomposes the PVK structure.[267] Currently, many reported that the performance of PVK QD films can benefit from the FAI post-treatment, but the hygroscopic FAI can exacerbates the degradation in the device when exposed to moisture.[268] Additionally, some PVK materials are fragile under the stress of light and oxygen, where the generated excitons can react with molecular oxygen to form superoxide and result in the decomposition of PVK materials.[269] Moreover, it is well-known that thermal stresses have a great impact on the structure and phase stability of PVK materials.[270] For $FAPbI_3$ perovskite which is widely applied in QDs, it can exhibit two different phases including a yellow hexagonal phase and a black trigonal phase. Under thermal stress, the $FAPbI_3$ can transit between these two phases showing phase instability.[265] Due to the volatile nature, the organic component in PVK can decompose and escape from the lattice to degrade the device under the environmental stressors.[268,271] For extensively studied all-inorganic PVK QDs, they have good resistance to oxygen and moisture as there are no organic cations. However, all-inorganic PVK materials suffer from a notorious phase instability issue, namely, the black perovskite phase can quickly degrade to a non-perovskite yellow phase, thus deteriorating the device performance even under room temperature.[272,273]

Fortunately, PVK QDs show better phase stability than PVK bulk materials because the tensile surface strain induced by ligands on PVK QDs can stabilize the perovskite phase and resist the crystal distortion.[237] Recent studies proved that $CsPbI_3$ QDs can maintain the stable perovskite phase after storage in ambient for hundreds of hours.[145] Luther and coworkers demonstrated that the degradation of $CsPbI_3$ QDs is 2 orders of magnitude slower than the $CsPbI_3$ bulk film.[274] In addition, they reported that the compositional instability of $CsPbI_3$ QDs is dominant, where surface defect states initiate and accelerate the oxidation of QDs to form superoxide and other oxidants. It is well recognized in the community that the complicated structural and phase degradation remains an obstacle for PVK QDs. Furthermore, compared to PbX QDs, PVK QDs suffer from different degradation routes caused by their unique ion migration and phase separation behaviors. Some ions in PVK own low activation energies, for example, 0.84 eV for MA^+ and the 0.58 eV for I^-, and can easily migrate under external stimulation.[275,276] When being exposed to illumination, heat or electric field, those ions can be redistributed and even form undesired phases in PVK to degrade the device performance.[277] Along with the migrated ions, defects such as vacancies and interstitials can be created and aggravate the ion migration.[278] Compared to bulk PVK materials, using some capping ligands, such as KBr, in PVK QDs is an effective method to suppress the ion migration, where those ligands can passivate the surface defects of PVK QDs and thus mitigating the pathways of ion migration.[46,279]

Apart from the intrinsic instability of QDs, other device components including carrier transport layers (CTLs) and electrodes which are essential for both PbX and PVK QD solar cells, can cause the instability of PV devices. For instance, zinc oxide (ZnO) and titanium oxide (TiO_2), the widely used CTLs in QD solar cells, show photo-instability behaviors.[221,227] Kim and coworkers proved that the ZnO CTL can degrade and cause energetic disorder in solar cells under illumination.[280] Choi and coworkers reported that the TiO_2 CTL, due to its vigorous photocatalytic property, can facilitate the phase degradation of $CsPbI_3$ QDs.[281] The degradation induced by electrodes also limits the device lifetime. Domanski and coworkers reported that the commonly used electrode gold (Au) can diffuse into other layers under thermal stresses, causing irreversible degradation for solar cells.[282] Moreover, it is worth mentioning that the operational stability of the device governs the actual lifetime.[283] Unlike environmental stress such as oxygen and moisture which can be prevented by encapsulation, operational stress is unavoidable for solar cells. Besides light illumination, the electrical field induced by the operational load accelerates the degradation of the device for both types of QD solar cells.

© 2021 Wiley-VCH GmbH

For instance, an electric field can cause a "poling effect" to the device and accelerate the ion migration of PVK, which directly reduces the build-in potential of the solar cells and hinders the charge transport.[284]

4.2. Strategies to Improve the Device Stability

Recently, an increasing number of studies have focused on solving the stability issue of PVK solar cells. Owing to tremendous efforts, a remarkable lifetime of over 1100 h under illumination has been proved for QD solar cells.[127] Regarding the instability of dynamic QD surfaces, several passivation strategies have been developed to eliminate the degradation sources for both types of QD solar cells. The formation of dangling bonds and the diffusion of oxidants can be prevented by the ligand exchange methods. When using short ligands such as *n*-alkythiolate, the packing density of QD films can be increased with a smaller QD size to improve QD stability.[285] For both PbX and PVK QDs, passivation with halide species is a useful strategy to improve device stability. By using PbX_2 (X = I, Br, or Cl) as the passivation source, the device lifetime of PbS QD solar cells under ambient can be extended to over 1000 h.[168] When passivated with dodecyldimethylammonium bromide (DDAB), the Br^- ion from DDAB can deactivate the Br^- vacancies on the $CsPbBr_3$ QD surface and increase the stability of QDs.[286]

On the other hand, it is worth mentioning that passivation strategies for PbX and PVK QDs are very different due to the different ionic structures and surface energies. Besides halide species passivation, cadmium passivation, P-O-moieties passivation, and core/shell passivation are well-established strategies for improving the stability of PbX QDs.[17,250,287] The undesirable oxidation can be leveraged to improve the stability of PbS QDs, where the partial oxidation of the PbS surface creates Fermi level pinning and raises the Schottky barrier to enhance the light stability.[249] Recently, Sargent and coworkers introduced additional potassium iodide (KI) on the surface of PbS QDs, which can act as a shield to prevent QDs oxidation.[288] As a result, they demonstrated PbS QD solar cells exhibiting improved operational stability, which maintained over 80% of its initial PCE after operation at maximum power point (MPP) for 300 h. Using a similar approach, Huang and coworkers applied potassium triiodide (KI_3) combined with PbX_2 matrix as surface ligands on PbS QDs and demonstrated remarkable operational stability of QD solar cells.[253] After the continuous operation at MPP for 20 h, their fabricated device maintained 94% of its initial PCE of 12.1%. For PVK QDs, effective passivation is needed to eliminate the ionic surface degradation sources. Yu and coworkers reported the use of poly(ethylene oxide), while Xu and coworkers proved the use of phosphoric acids (PAs), to passivate the methylammonium lead bromide ($MAPbBr_3$) QDs.[289,290] Both methods are based on organic materials, which reduced the defects caused by the ionic bonding of PVK QDs and enhanced the device stability. Ling and coworkers introduced various inorganic sulphonium salts to passivate the $CsPbI_3$ QDs, and Zhang and coworkers used metal ion-based ligands to passivate the $CsPbBr_3$ QDs.[160,291] These inorganic passivation methods can effectively fill the vacancies of the QD surface and improve the QD stability.

Regarding the unique structural and phase instability of PVK QDs, doping and compositional engineering are viable solutions. Over the past years, there have been studies focusing on improving the stability of PVK bulk materials by optimizing their composition and introducing effective dopants.[292–294] Similarly, Mn^{2+} has been used to stabilize the black perovskite phase of $CsPbX_3$QDs.[295–297] The Mn^{2+} dopant effectively tunes the surface and lattice energy of $CsPbX_3$ QDs, shrinking the lattice to maintain a stable phase. Liu and coworkers enhanced the moisture stability of PVK QDs by optimizing the composition of Sn^{2+} in the $CsPb_{1-x}Sn_xIBr_2$ QDs.[298] Ma and coworkers employed Yb^{3+} doping in $CsPbI_3$ QDs and reported improved storage stability of the fabricated solar cells.[191] They demonstrated that Yb^{3+} lanthanide cations can reduce the lattice defects and surface vacancies in $CsPbI_3$ QDs. Recently, Jen and coworkers used ZnI_2 as the dopant in $CsPbI_3$ QDs and revealed that the doping of Zn^{2+} can improve the thermal stability of the device by increasing the formation energy and the Goldschmidt tolerance factor of $CsPbI_3$ QDs.[299] Regarding PV devices, several strategies have been reported to solve the degradation issue caused by interfaces, CTLs, and electrodes. For example, the stability of ZnO CTLs can be improved by various types of dopants, such as aluminum, magnesium, and cesium.[226,300] Using bilayer structured or self-assembled monolayer-treated CTLs is another effective method to increase the device stability.[301,302] Recently, Choi and coworkers replaced TiO_2 with chloride-passivated SnO_2 as CTL in the $CsPbI_3$ QD solar cells and proved that the operational stability of the device can be significantly improved.[281] As a result, their fabricated devices without encapsulation maintained 80% of their initial PCE after test under one-sun illumination in the air for 8 h. On the other hand, encapsulation that prevents the penetration of oxygen and moisture is a valid method for QD solar cells to achieve good stability. Capping layers such as TeO_2 and MgF_2, which have been widely applied in silicon, perovskite, and OSCs, can be used for encapsulating QD solar cells.[162,303]

Figure 7 depicts the progress of stability improvement of QD solar cells in the last 10 years, and the corresponding works are summarized in **Table 2**. The PCE merits, which are defined as the maintained PCE after the stability test, are used as intuitive parameters to evaluate the stability of QD solar cells. As shown in Figure 7, many PbX and PVK QD solar cells have been reported with high shelf stability. Baek and coworkers fabricated PbS QD solar cells with remarkable air stability, which maintained 90% of its initial PCE after storage in air for 180 days.[228] Liu and coworkers reported the $CsPbI_3$ QD solar cell with only 2% PCE degradation after storage in air for 90 days.[238] In comparison, fewer studies have been focused on the light and operational stability of the devices. Many QD solar cells show fast degradation under illumination conditions. As the illumination and the electric field are inevitable for solar cell operation, the light and operational stability of both PbX and PVK QD solar cells needs more investigation and improvement. Moreover, it is worth mentioning that current publications still lack consistency in the stability measurements, which makes the comparison between different works challenging. For future endeavors, the consensus statement in the International Summit on Organic Photovoltaic Stability (ISOS) protocols is suggested for benchmarking stability measurements.[304]

© 2021 Wiley-VCH GmbH

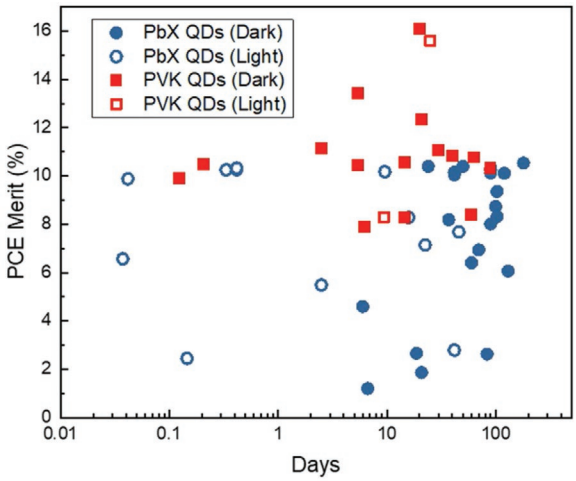

Figure 7. Stability of QD solar cells presented by the PCE merit versus device aging days. PCE merit is the retained PCE value of the device after the degradation. Results from the stability test involving illumination are represented by "Light," while results from the stability test under dark conditions are represented by "Dark." The figure is drawn based on data in Table 2.

5. Challenges and Outlooks of Quantum Dot Photovoltaic Technologies

5.1. Large-Scale Fabrication

To date, the large-scale fabrication of QD solar cells still faces many challenges which hinder their commercialization. One of the obstacles is the inefficient QDs synthesis process.[316] Currently most researchers adapt a lab-scale hot-injection strategy to synthesize monodisperse QDs, which has a short reaction time (<10 min) and a low production (<100 mg yield).[101,317,318] To overcome this challenge, it is desirable to develop simple QD synthesis protocols, obtaining high reproducibility, high QDs quality, and high yield. Furthermore, many widely applied QD synthesis strategies rely on the use of organic ligands with long-alkyl chains in the precursor, which then needs a tedious ligand exchange step to improve the quality of QD films.[21,101] As mentioned, the SPLE strategy with pre-exchanged QD inks is preferred for large-scale fabrication. Recently, Ma and coworkers developed a direct one-step synthesis method for iodide-capped PbS QDs and compared their method with the conventional one.[319] Besides the simplicity, the team proved that the cost of their one-step method could be significantly reduced from 16 \$ g^{-1} of the conventional method to 6 \$ g^{-1}.

In the context of QD film fabrication, most QD solar cells are reported in small sizes with active area <1 cm^2 by using lab-scale fabrication methods, such as spin-coating and drop-casting techniques. Scaling up the device fabrication remains a great challenge for the application and commercialization of QD solar cells.[249] The lab-scale methods are incompatible with large-area fabrication, as they can easily cause low-quality film with non-uniformity. In addition, most of the lab-scale fabrication is time- and material-consuming.[225,320] For example, the LBL coating method for thick QD films requires multiple depositions and washing steps, which results in high material consumptions.[321] In this sense, developing large-scale fabrication methods with simple processing, low-cost, and high uniformity, is desirable for advancing QD solar cells. Inkjet printing, spray coating, slot-die coating, and blade coating are four widely used large-scale fabrication methods for fabricating QD-based optoelectronic devices.[249] The inkjet printing method uses nozzles to deposit a large-area QD film, where the film uniformity is controlled by the viscosity of solvents and the processing time. Compared to spin coating and drop casting, inkjet printing reduces material consumption, leading to a lower cost. However, the ink solvent's uneven evaporation can cause a coffee-ring effect for the deposited film.[322] The spray coating method uses a nozzle with high pressurized gas to deposit QD films, where the gas pressure simply controls the film uniformity. Compared to other methods, the spray coating method shows superior air-process ability, and an inert gas atmosphere is not required for the film fabrication.[323] Using the spray coating method, Kramer and coworkers have successfully obtained a PCE of 8.1% for PbS QD solar cells.[324] The slot-die coating or blade coating method uses a dispenser head or a knife for spreading the QD inks to deposit films, where the spreading speed controls the film uniformity and the knife to substrate distance controls the film thickness.[325] Kirmani and coworkers reported that the material consumption in slot-die coating or blade coating method is only 4% of the material consumption with the spin-coating method.[311] Using the blade coating method, a remarkable PCE of 10.3% has been obtained for PbS QD solar cells.[181] It is worth mentioning that spray coating, slot-die coating, and blade coating are compatible with a cost-efficient roll-to-roll fabrication process, which underscores their promising future for commercialization.[249] Unfortunately, the PCE of large-scale QD solar cells still lags behind the lab-scale counterparts. Surprisingly, to the best of our knowledge, there has been no report on fabricating PVK QD solar cells using any large-scale compatible processing methods. As the PCE of PVK QD solar cells has overtaken PbX QD solar cells, further intensive investigations on large-scale PVK QD solar cells can be envisioned in the field.

5.2. Lead Toxicity

Although both PbX and PVK QDs have achieved tremendous progress in the past decade, the presence of lead, which is harmful to human health and the environment, raises concern on their practical applications. Fortunately, for solar cell application, a small amount of lead is allowed, since the solar panel is exempted from some legislations such as the European Restriction on Hazardous Substances (RoHS).[326,327] Nonetheless, when considering large-scale photovoltaic systems, the accumulated amount of lead is worrisome. Under this circumstance, lead-free QD solar cells may be viable solutions.[328,329] For example, In-based QDs such as InAs, Indium zinc phosphorus, and Indium antimonide, exhibiting a broad-range photo response from UV to NIR and high absorption coefficient, are considered promising alternatives to PbX QDs.[330] However, when applied in solar cells, In-based QDs show poor device performance than PbX QDs due to their poly-disperse of the QD size and poor QD surface passivation.[41,331] On the other research front, replacing Pb with other ions such as Tin (Sn),

© 2021 Wiley-VCH GmbH

Table 2. Stability data of some representative QD solar cells. (room temperature (RT), relative humidity (RH), without (w/o), and not available (n/a)).

Year	Device structure	PCE	Test condition				PCE Merit	Ref.
			Light	Thermal	Air (RH humidity)	Time		
PbX QD								
2010	ITO/ZnO/PbS/Au	2.94%	One-sun	RT	Air (n/a)	1000 h	2.79%	[305]
2010	ITO/PbS/LiF/Al/Ag	2.00%	w/o	RT	Air (n/a)	160 h	1.20%	[306]
2011	FTO/TiO_2/PbS-TBAI/Au/Ag	5.54%	w/o	RT	Dry air (n/a)	6 days	4.60%	[210]
2012	ITO/PbS/PbS-Ag/AZO/Ag	6.10%	One-sun	RT	n/a	60 h	5.49%	[300]
2013	ITO/ZnO/PbS-TBAI/PbS-EDT/MoO_x/Al	8.55%	w/o	RT	Air (n/a)	37 days	8.19%	[94]
2014	ITO/PbS/LiF/Al/Ag	3.39%	w/o	RT	Air (n/a)	500 h	1.86%	[307]
2014	FTO/PEI/PbS/MoO_3/Au/Ag	3.80%	w/o	RT	Air (n/a)	450 h	2.66%	[308]
2015	FTO/TiO_2/PbSe–PbI_2/PbSe-MPA/Au	6.47%	w/o	RT	Air (n/a)	60 days	6.41%	[309]
2015	FTO/ZnO/TiO_2/PbS/Au	6.13%	w/o	RT	Air (n/a)	130 days	6.07%	[301]
2016	FTO/TiO_2/PbSe/Au	3.50%	w/o	RT	Air (n/a)	2000 h	2.63%	[310]
			One-sun	RT	Air (n/a)	3.5 h	2.45%	
2016	ITO/ZnO/PbS-I/PbS-EDT/MoO_3/Au/Ag	9.60%	One-sun	60 °C	N_2	1100 h	7.68%	[127]
2016	ITO/ZnO/PbS-TBAI/PbS-EDT/GD/Al	10.64%	w/o	RT	Air (n/a)	120 days	10.11%	[178]
2017	ITO/ZnO/PbS-PbX_2-AA/PbS-EDT/Au	11.28%	w/o	RT	Air (n/a)	1000 h	10.15%	[168]
2017	ITO/IZO/PbS-TBAI/PbS-EDT/Au/TeO_2	7.30%	w/o	RT	Air (n/a)	70 days	6.94%	[303]
			One-sun	RT	Air (n/a)	0.9 h	6.57%	
2017	ITO/MZO/PbS-TBAI/PbS-EDT/Au	10.40%	w/o	RT	Air (n/a)	103 days	9.36%	[226]
			One-sun	RT	Air (n/a)	1 h	9.88%	
2017	ITO/ZnO-JTCA/PbS-PDMII/PbS-PDT/Au	10.83%	w/o	RT	Air (n/a)	24 days	10.40%	[221]
			One-sun	RT	Air (n/a)	4.5 h	10.50%	
2018	ITO/ZnO-K/PbS-I/PbS-PDT/Au	10.80%	w/o	RT	Air (n/a)	90 days	10.26%	[227]
			One-sun	RT	Air (n/a)	10 h	10.26%	
2018	ITO/ZnO/PbS–PbI_2/PbS-EDT/Au	11.00%	w/o	RT	Air (n/a)	356 days	7.70%	[311]
2018	ITO/MZO/PbS-PbX_2/PbS-EDT/Au/MgF_2	8.40%	w/o	RT	Air (n/a)	103 days	8.32%	[162]
			One-sun	RT	Air (n/a)	540 h	7.14%	
2018	ITO/CsZnO/PbS-TBAI/PbS-EDT/Au	10.43%	w/o	RT	Air (n/a)	90 days	10.12%	[312]
2018	ITO/ZnO/n-PbS/p-PbS/Au	10.91%	w/o	RT	Air (n/a)	100 days	8.73%	[181]
2018	ITO/ZnO-EAL/PbS-I/PbS-PDT/Au	10.75%	w/o	RT	Air (40 ± 3%)	90 days	10.32%	[227]
			One-sun	45 ± 2 °C	Air (40 ± 2%)	10 h	10.32%	
2018	ITO/ZnO/PbS-I/PbS-MPA/p-MeO-TPD/Ag	11.71%	w/o	RT	Air (n/a)	180 days	10.54%	[228]
2019	ITO/ZnO/PbS-TBAI/PbS-EDT/Au	8.90%	w/o	RT	Air (50%)	90 days	8.01%	[313]
2019	ITO/ZnO/PbS-TBAI/PbS-EDT/Au	10.60%	One-sun	RT	N_2	230 h	10.18%	[314]
2019	ITO/ZnO/PbS/PbS-EDT/Au	11.18%	w/o	RT	Air (n/a)	50 days	10.40%	[163]
2019	ITO/ZnO/PbSe-PbI_2/PbS-EDT/Au	10.68%	w/o	RT	Air (>50%)	1000 h	10.04%	[232]
			One-sun	RT	Air (>50%)	8 h	10.25%	
2020	ITO/ZnO/PbS-FABr/PbS-EDT/Au	13.80%	One-sun	RT	N_2	380 h	8.28%	[315]
2020	ITO/ZnO/KPbS/PbS-EDT/Au	12.60%	One-sun	RT	Air (50 ± 10%)	300 h	10.08%	[288]
2020	ITO/ZnO/PbS-PbX_2-KI_3/PbS-EDT/Au	12.10%	One-sun	RT	Air (na)	20 h	11.20%	[253]
PVK QD								
2016	FTO/TiO_2/$CsPbI_3$/Spiro-OMeTAD/MoOx/Al	10.77%	w/o	RT	N_2	64 days	10.77%	[70]
2018	FTO/TiO_2/μGR-$CsPbI_3$/PTAA/Au	11.64%	w/o	RT	N_2	30 days	11.06%	[157]
			w/o	RT	Air (60%)	5 h	10.48%	
			w/o	100 °C	N_2	3 h	9.89%	
2018	ITO/TiO_2/$CsPbI_2Br$/P3HT/Au	12.02%	w/o	RT	N_2	960 h	10.82%	[236]
2018	ITO/SnO_2/$FAPbI_3$/Spiro-OMeTAD/Au	8.38%	w/o	RT	Air (n/a)	60 days	8.38%	[237]
			One-sun	RT	Air (n/a)	226 h	8.29%	

© 2021 Wiley-VCH GmbH

Table 2. Continued.

Year	Device structure	PCE	Test condition				PCE Merit	Ref.
			Light	Thermal	Air (RH humidity)	Time		
2019	FTO/TiO_2/$CsPbI_3$/Spiro-OMeTAD/Au	12.15%	w/o	RT	Air (<20%)	90 days	10.33%	[238]
2019	FTO/TiO_2/$CsPbI_3$:Yb/PTB7/MoO_x/Ag	13.12%	w/o	RT	Air (20–30%)	150 h	7.87%	[191]
2019	ITO/PTAA/$CsPbI_3$/C60/BCP/Cu	13.40%	w/o	RT	Air (n/a)	500 h	12.33%	[239]
2020	ITO/SnO_2/$Cs_{0.5}FA_{0.5}PbI_3$/Spiro-OMeTAD/Au	16.60%	w/o	RT	Air (50–70%)	20 days	16.10%	[46]
			One-sun	50–65 °C	N_2	600 h	15.60%	
2020	FTO/TiO_2/$CsPbI_3$/PBDB-T	13.80%	w/o	RT	Air (20–30%)	350 h	8.28%	[145]
	FTO/TiO_2/$FAPbI_3$/PBDB-T	13.20%	w/o	RT	Air (20–30%)	350 h	10.56%	
2020	FTO/TiO_2/$CsPbI_3$/PTAA/MoO_x/Ag	14.90%	w/o	RT	Dry air (n/a)	130 h	13.41%	[145]
			w/o	RT	Air (30–40%)	130 h	10.43%	
2020	FTO/TiO_2/$CsPbI_3$/PbSe/Spiro-OMeTAD/Ag	13.90%	w/o	RT	Air (40%)	60 h	11.12%	[90]
2020	FTO/TiO_2/$CsPbI_3$/Spiro-OMeTAD/MoO_x/Ag	16.07%	w/o	RT	Air (20–30%)	10 days	13.68%	[299]
2021	FTO/Cl-SnO2/$CsPbI_3$/Spiro-OMeTAD/MoO_x/Ag	14.50%	One-sun	RT	Air (50%)	8 h	11.60%	[281]

Germanium (Ge), Copper (Cu), and Bismuth (Bi) is an effective way to produce lead-free PVK materials.[332–334] This composition engineering strategy has also attracted attention in the field of QDs, and lead-free PVK QD based LEDs and detectors have become hot research topics.[335–337] Lead-free PVK solar cells have achieved some developments in the past 5 years with the PCE surpassing 10%, while there has been no report on lead-free PVK QD solar cells.[332,338] Regarding solar cell applications, lead-free PVK QDs may have a greater potential over other lead-free QD materials and deserve more investigations. Overall, the research on lead-free QD solar cells is still in its infancy stage, warranting more effort and development.

6. Conclusion and Outlook

QD solar cells, benefiting from quantum confinement and MEG effects, have shown unique advantages absent in other types of solar cells. To date, most Pb-based high-performance devices are derived from two main classes of materials: PbX and PVK QDs. The tale of these two materials will continue playing out in the arena of photovoltaics. In the context of PV applications, PVK QDs have emerged as a rising star in the field, while both PbX and PVK QD solar cells still have significant room to be improved. In this review, we comparatively summarized and discussed these two types of QD solar cells, with a focus on fundamental photophysics, device structures, and photovoltaic performance. Generally, PbX and PVK QDs and their corresponding PV devices share many similarities, but they also exhibit many differences, as summarized in **Table 3**. By comparing the unique characteristics of these two classes of prominent nanomaterials, in-depth understandings of QD solar cells are expected to facilitate the realization of the potential of QD solar cells.

Regarding the QD physics, PbX QDs provide potential advantages over PVK QDs for their stronger quantum confinement effect, controllable band shifting, and lower MEG threshold energy. On the other hand, PVK QDs own superiority in high defect tolerance and diverse compositions than PbX QDs. In the context of photovoltaic device engineering, surface ligand exchange of PVK QDs is lagging far behind PbX QDs from perspectives of ligands diversity and sophistication. It is of great necessity to develop a more efficient approach for the removal of native ligands in PVK QD solar cells, which is expected to

Table 3. A high-level comparison of PbX QDs and PVK QDs.

	PbX QDs	PVK QDs
Crystal structure	Cubic structure with S or Se atoms located at octahedral interstices of the face-centered sub-lattice of Pb atoms	Perovskite structure (orthorhombic, tetragonal, and cubic in different temperature regimes)
Composition	PbS, PbSe, PbS_xSe_{1-x}	ABX_3 (e.g., A = MA^+, FA^+, or Cs^+; B = Pb^{2+} or Sn^{2+}; X = Cl^-, I^- or Br^-)
Quantum confinement effects	Strong	Weak
Bandgap tuning	Varying QD size	Varying QD size and compositional engineering
Defect tolerance	Low	High
Multiple exciton generation	Low threshold	High threshold
Surface chemistry ligands	BT, 1,3-BDT, 1,2-BDT, 1,4-BDT, EDT, EDA, MPA, TBAX, etc.	MeOAc, FA, PEA, GA, Glycine, L-PHE, CsOAc, NaAc, etc.
Photovoltaic device structure	Schottky, depleted heterojunction, P-N/P-i-N junction, quantum homojunction, and bulk heterojunction	N-i-P junction, P-i-N junction, and heterojunction
Stability issues	Dynamic QD surfaces	Dynamic QD surfaces, structural and phase instability, and ion migration
Record PCE	13.8%	16.6%

© 2021 Wiley-VCH GmbH

further enhance the carrier transport process. Additionally, due to their exceptionally diverse chemical compositions, PVK QDs provide a facile way to fabricate multiple layers and quantum junction solar cells than PbS QDs, which warrants more research efforts. From the perspective of photovoltaic device stability, both PbX and PVK QDs suffer from the instability caused by dynamic QD surfaces, thus requiring high-level surface passivation for stable devices. Due to the feature of low defect tolerance, the degradation of PbX QDs is more sensitive to QD surface changes than PVK QDs. However, PVK QDs suffer from structural stability issues and ion migration induced degradation, which need to be solved. Owing to fast developments in various stability improvement strategies, both PbX and PVK QD solar cells have already been reported with high shelf stability. However, their light stability and operational stability still need more investigations and improvements. Besides PCE and stability, for achieving the commercialization of QD solar cells, large-scale fabrication and lead toxicity are two major challenges. Developing large-scale fabrication methods with desirable features such as simple processing, low-cost, and high uniformity for QD solar cells is in pressing demand, and more endeavors are needed to develop lead-free PVK QD materials for PV applications.

Meanwhile, it is worth noting that the unique properties of PbX and PVK QDs should be fully exploited and properly utilized. In this context, we suggest several promising research directions to further advancing QD solar cells: i) Investigating the surface chemistry of PVK QDs is the priority to improve the PV device performance of PVK QD solar cells. Great efforts have been delivered to explore the surface chemistry and ligand exchange methods for PbX QDs, while understanding of PVK QDs is lagging behind. Surface chemistry strategies for PbX and PVK QDs are very different due to their distinct ionic structures and surface energies. Also, surface chemistry strategies for PVK QDs can be more diverse than PbX QDs. Therefore, efforts on developing suitable surface treatments for PVK QDs are warranted. ii) Designing band-aligned tandem QD solar cells is a promising direction. Both PbX and PVK QDs exhibit diverse bandgap tuning properties, making the band matching of tandem QD solar cells very flexible. The mid bandgap of PVK QDs and their high open-circuit voltage due to defect tolerance make them ideal for the top cell in tandem devices, while the narrow bandgap of PbX QD with strong NIR light absorption makes them suitable for the bottom cell. All-QD tandem solar cells consisting of both PbX and PVK QDs are expected to deliver higher PCE than the single-junction QD solar cells. iii) PbX QD/PVK QD heterostructure solar cell is another promising way to realize the potential of QD solar cells. Unlike tandem devices, heterostructure QD solar cells consist of stacked two QD layers without the interconnection layer. When stacking mid-bandgap PVK QDs and narrow-bandgap PbX QDs together to fabricate solar cells, a stronger light absorption, as well as, better device performance, are expected. iv) Combining QDs with other types of solution-processed solar cells, such as, OSCs and PSCs may produce high-performance PV devices. The organic polymer can have a passivation effect on QDs, while QDs can increase the charge transfer between polymers. The mutual beneficial effect between QDs and other active materials is expected to produce composites with enhanced optoelectronic properties and thus results in optimal PV performance. Moreover, as QD materials have been widely recognized to offer superior semitransparency and mechanical flexibility, future research on semitransparent and flexible QD solar cells is recommended to explore more diverse applications for QDs.

Acknowledgements

L.D. and L.H. contributed equally to this work. J.Y. would like to thank the support from National Key Research and Development Program of China (No. 2019YFE0108600), National Natural Science Foundation of China (No. 52073198, 51803144), and the Collaborative Innovation Center of Suzhou Nano Science and Technology, Soochow University. T.W. acknowledges the support from the Australian Research Council (DP190103316).

Conflict of Interest

The authors declare no conflict of interest.

Keywords

lead chalcogenides, perovskite quantum dots, photovoltaics, solar cells, stability

Received: January 30, 2021
Revised: March 21, 2021
Published online: April 17, 2021

[1] A. Ingenito, G. Nogay, Q. Jeangros, E. Rucavado, C. Allebé, S. Eswara, N. Valle, T. Wirtz, J. Horzel, T. Koida, M. Morales-Masis, M. Despeisse, F.-J. Haug, P. Löper, C. Ballif, *Nat. Energy* **2018**, *3*, 800.
[2] R. V. K. Chavali, S. De Wolf, M. A. Alam, *Prog. Photovoltaics* **2018**, *26*, 241.
[3] J. Y. Kim, J.-W. Lee, H. S. Jung, H. Shin, N.-G. Park, *Chem. Rev.* **2020**, *120*, 7867.
[4] E. H. Jung, N. J. Jeon, E. Y. Park, C. S. Moon, T. J. Shin, T.-Y. Yang, J. H. Noh, J. Seo, *Nature* **2019**, *567*, 511.
[5] M. L. Petrus, J. Schlipf, C. Li, T. P. Gujar, N. Giesbrecht, P. Müller-Buschbaum, M. Thelakkat, T. Bein, S. Hüttner, P. Docampo, *Adv. Energy Mater.* **2017**, *7*, 1700264.
[6] A. Uddin, M. B. Upama, H. Yi, L. J. C. Duan, *Coatings* **2019**, *9*, 65.
[7] A. Wadsworth, M. Moser, A. Marks, M. S. Little, N. Gasparini, C. J. Brabec, D. Baran, I. J. C. S. R. McCulloch, *Chem. Soc. Rev.* **2019**, *48*, 1596.
[8] R. Xue, J. Zhang, Y. Li, Y. Li, *Small* **2018**, *14*, 1801793.
[9] H. Lee, H.-J. Song, M. Shim, C. J. E. Lee, *Energy Environ. Sci.* **2020**, *13*, 404.
[10] J. Yuan, A. Hazarika, Q. Zhao, X. Ling, T. Moot, W. Ma, J. M. Luther, *Joule* **2020**, *4*, 1160.
[11] T. Blachowicz, A. J. A. S. Ehrmann, *Appl. Sci.* **2020**, *10*, 1743.
[12] Y. Zhang, G. Wu, F. Liu, C. Ding, Z. Zou, Q. Shen, *Chem. Soc. Rev.* **2020**, *49*, 49.
[13] Z. Hens, I. Moreels, *J. Mater. Chem.* **2012**, *22*, 10406.
[14] H. Meddeb, N. Osterthun, M. Götz, O. Sergeev, K. Gehrke, M. Vehse, C. Agert, *Nano Energy* **2020**, *76*, 105048.

© 2021 Wiley-VCH GmbH

[15] G. Heather, C. J. Tom, J. L. K. D. Nathaniel, L. B. Marcus, *Nanophotonics* **2018**, *7*, 111.
[16] O. E. Semonin, J. M. Luther, S. Choi, H.-Y. Chen, J. Gao, A. J. Nozik, M. C. Beard, *Science* **2011**, *334*, 1530.
[17] J. Zhang, J. Gao, C. P. Church, E. M. Miller, J. M. Luther, V. I. Klimov, M. C. Beard, *Nano Lett.* **2014**, *14*, 6010.
[18] L. Hu, Q. Zhao, S. Huang, J. Zheng, X. Guan, R. Patterson, J. Kim, L. Shi, C.-H. Lin, Q. Lei, D. Chu, W. Tao, S. Cheong, R. D. Tilley, A. W. Y. Ho-Baillie, J. M. Luther, J. Yuan, T. Wu, *Nat. Commun.* **2021**, *12*, 466.
[19] X. Zhang, Y. Qian, X. Ling, Y. Wang, Y. Zhang, J. Shi, Y. Shi, J. Yuan, W. Ma, *ACS Appl. Mater. Interfaces* **2020**, *12*, 27307.
[20] Y. Yin, A. P. Alivisatos, *Nature* **2005**, *437*, 664.
[21] M. A. Boles, D. Ling, T. Hyeon, D. V. Talapin, *Nat. Mater.* **2016**, *15*, 141.
[22] J. J. Storhoff, A. A. Lazarides, R. C. Mucic, C. A. Mirkin, R. L. Letsinger, G. C. Schatz, *J. Am. Chem. Soc.* **2000**, *122*, 4640.
[23] C. P. Byers, H. Zhang, D. F. Swearer, M. Yorulmaz, B. S. Hoener, D. Huang, A. Hoggard, W.-S. Chang, P. Mulvaney, E. Ringe, N. J. Halas, P. Nordlander, S. Link, C. F. Landes, *Sci. Adv.* **2015**, *1*, e1500988.
[24] A. Badawi, N. Al-Hosiny, S. Abdallah, S. Negm, H. Talaat, *Sol. Energy* **2013**, *88*, 137.
[25] S.-C. Pu, M.-J. Yang, C.-C. Hsu, C.-W. Lai, C.-C. Hsieh, S. H. Lin, Y.-M. Cheng, P.-T. Chou, *Small* **2006**, *2*, 1308.
[26] D. V. Talapin, C. B. Murray, *Science* **2005**, *310*, 86.
[27] J. Gao, J. M. Luther, O. E. Semonin, R. J. Ellingson, A. J. Nozik, M. C. Beard, *Nano Lett.* **2011**, *11*, 1002.
[28] M. Yuan, M. Liu, E. H. Sargent, *Nat. Energy* **2016**, *1*, 16016.
[29] P. R. Brown, D. Kim, R. R. Lunt, N. Zhao, M. G. Bawendi, J. C. Grossman, V. Bulović, *ACS Nano* **2014**, *8*, 5863.
[30] G. Konstantatos, I. Howard, A. Fischer, S. Hoogland, J. Clifford, E. Klem, L. Levina, E. H. Sargent, *Nature* **2006**, *442*, 180.
[31] L. Sun, J. J. Choi, D. Stachnik, A. C. Bartnik, B.-R. Hyun, G. G. Malliaras, T. Hanrath, F. W. Wise, *Nat. Nanotechnol.* **2012**, *7*, 369.
[32] V. L. Colvin, M. C. Schlamp, A. P. Alivisatos, *Nature* **1994**, *370*, 354.
[33] N. Tessler, V. Medvedev, M. Kazes, S. Kan, U. Banin, *Science* **2002**, *295*, 1506.
[34] Y. Zhu, Y. Mu, F. Tang, P. Du, H. Ren, *Front. Optoelectron.* **2020**, *13*, 291.
[35] V. I. Klimov, *Annu. Rev. Condens. Matter Phys.* **2014**, *5*, 285.
[36] M. L. Böhm, T. C. Jellicoe, M. Tabachnyk, N. J. L. K. Davis, F. Wisnivesky-Rocca-Rivarola, C. Ducati, B. Ehrler, A. A. Bakulin, N. C. Greenham, *Nano Lett.* **2015**, *15*, 7987.
[37] A. Rao, R. H. Friend, *Nat. Rev. Mater.* **2017**, *2*, 17063.
[38] M. Li, R. Begum, J. Fu, Q. Xu, T. M. Koh, S. A. Veldhuis, M. Grätzel, N. Mathews, S. Mhaisalkar, T. C. Sum, *Nat. Commun.* **2018**, *9*, 4197.
[39] S. A. Mann, R. R. Grote, R. M. Osgood, A. Alù, E. C. Garnett, *ACS Nano* **2016**, *10*, 8620.
[40] D. Hahm, D. Ko, B. G. Jeong, S. Jeong, J. Lim, W. K. Bae, C. Lee, K. Char, *J. Inf. Disp.* **2019**, *20*, 61.
[41] R. W. Crisp, N. Kirkwood, G. Grimaldi, S. Kinge, L. D. A. Siebbeles, A. J. Houtepen, *ACS Appl. Energy Mater.* **2018**, *1*, 6569.
[42] M. Bernechea, N. C. Miller, G. Xercavins, D. So, A. Stavrinadis, G. Konstantatos, *Nat. Photonics* **2016**, *10*, 521.
[43] Z. Liu, J. Yuan, S. A. Hawks, G. Shi, S.-T. Lee, W. Ma, *Sol. RRL* **2017**, *1*, 1600021.
[44] J. S. Shaikh, N. S. Shaikh, S. S. Mali, J. V. Patil, S. A. Beknalkar, A. P. Patil, N. L. Tarwal, P. Kanjanaboos, C. K. Hong, P. S. Patil, *ChemSusChem* **2019**, *12*, 4724.
[45] L. Hu, R. J. Patterson, Z. Zhang, Y. Hu, D. Li, Z. Chen, L. Yuan, Z. L. Teh, Y. Gao, G. J. Conibeer, S. Huang, *J. Mater. Chem. C* **2018**, *6*, 731.
[46] M. Hao, Y. Bai, S. Zeiske, L. Ren, J. Liu, Y. Yuan, N. Zarrabi, N. Cheng, M. Ghasemi, P. Chen, M. Lyu, D. He, J.-H. Yun, Y. Du, Y. Wang, S. Ding, A. Armin, P. Meredith, G. Liu, H.-M. Cheng, L. Wang, *Nat. Energy* **2020**, *5*, 79.
[47] M.-J. Choi, F. P. G. de Arquer, A. H. Proppe, A. Seifitokaldani, J. Choi, J. Kim, S.-W. Baek, M. Liu, B. Sun, M. Biondi, B. Scheffel, G. Walters, D.-H. Nam, J. W. Jo, O. Ouellette, O. Voznyy, S. Hoogland, S. O. Kelley, Y. S. Jung, E. H. Sargent, *Nat. Commun.* **2020**, *11*, 103.
[48] D. A. Hines, P. V. Kamat, *ACS Appl. Mater. Interfaces* **2014**, *6*, 3041.
[49] S. Yin, (Thesis) Achieving High-Performance Infrared Range (IR) Photodiode via Bilayer Lead Sulfide Quantum, Master of Science dissertation, Carolina State University **2018**.
[50] M. Zhao, R. Peng, Q. Zheng, Q. Wang, M.-J. Chang, Y. Liu, Y.-L. Song, H.-L. Zhang, *Nanoscale* **2015**, *7*, 9268.
[51] G. E. Eperon, S. D. Stranks, C. Menelaou, M. B. Johnston, L. M. Herz, H. J. Snaith, *Energy Environ. Sci.* **2014**, *7*, 982.
[52] X. Yuan, X. Hou, J. Li, C. Qu, W. Zhang, J. Zhao, H. Li, *Phys. Chem. Chem. Phys.* **2017**, *19*, 8934.
[53] M. Albaladejo-Siguan, D. Becker-Koch, A. D. Taylor, Q. Sun, V. Lami, P. G. Oppenheimer, F. Paulus, Y. Vaynzof, *ACS Nano* **2020**, *14*, 384.
[54] S. Chen, Y. j. Wang, Q. Liu, G. Shi, Z. Liu, K. Lu, L. Han, X. Ling, H. Zhang, S. Cheng, W. Ma, *Adv. Energy Mater.* **2018**, *8*, 1701194.
[55] B. Sun, A. Johnston, C. Xu, M. Wei, Z. Huang, Z. Jiang, H. Zhou, Y. Gao, Y. Dong, O. Ouellette, X. Zheng, J. Liu, M.-J. Choi, Y. Gao, S.-W. Baek, F. Laquai, O. M. Bakr, D. Ban, O. Voznyy, F. P. G. de Arquer, E. H. Sargent, *Joule* **2020**, *4*, 1542.
[56] R. Dalven, *Infrared Phys.* **1969**, *9*, 141.
[57] S. I. Sadovnikov, A. I. Gusev, A. A. Rempel', *JETP Lett.* **2009**, *89*, 238.
[58] H. Beygi, S. A. Sajjadi, A. Babakhani, J. F. Young, F. C. J. M. van Veggel, *Appl. Surf. Sci.* **2018**, *457*, 1.
[59] H. Lu, G. M. Carroll, N. R. Neale, M. C. Beard, *ACS Nano* **2019**, *13*, 939.
[60] J. Zhang, J. Gao, E. M. Miller, J. M. Luther, M. C. Beard, *ACS Nano* **2014**, *8*, 614.
[61] A. G. Midgett, J. M. Luther, J. T. Stewart, D. K. Smith, L. A. Padilha, V. I. Klimov, A. J. Nozik, M. C. Beard, *Nano Lett.* **2013**, *13*, 3078.
[62] F. W. Wise, *Acc. Chem. Res.* **2000**, *33*, 773.
[63] H. Wang, Z. Zhang, J. Yu, P.-C. Lin, C.-C. Chueh, X. Liu, S. Guang, S. Qu, W. Tang, *ACS Appl. Mater. Interfaces* **2020**, *12*, 21633.
[64] M. A. Green, E. D. Dunlop, D. H. Levi, J. Hohl-Ebinger, M. Yoshita, A. W. Y. Ho-Baillie, *Prog. Photovoltaics* **2019**, *27*, 565.
[65] J. Tang, D. Li, *Front. Optoelectron.* **2020**, *13*, 191.
[66] F. Li, S. Zhou, J. Yuan, C. Qin, Y. Yang, J. Shi, X. Ling, Y. Li, W. Ma, *ACS Energy Lett.* **2019**, *4*, 2571.
[67] J. Yuan, C. Bi, S. Wang, R. Guo, T. Shen, L. Zhang, J. Tian, *Adv. Funct. Mater.* **2019**, *29*, 1906615.
[68] E. M. Sanehira, A. R. Marshall, J. A. Christians, S. P. Harvey, P. N. Ciesielski, L. M. Wheeler, P. Schulz, L. Y. Lin, M. C. Beard, J. M. Luther, *Sci. Adv.* **2017**, *3*, eaao4204.
[69] R. F. Kahwagi, S. T. Thornton, B. Smith, G. I. Koleilat, *Front. Optoelectron.* **2020**, *13*, 196.
[70] A. Swarnkar, A. R. Marshall, E. M. Sanehira, B. D. Chernomordik, D. T. Moore, J. A. Christians, T. Chakrabarti, J. M. Luther, *Science* **2016**, *354*, 92.
[71] D. N. Dirin, L. Protesescu, D. Trummer, I. V. Kochetygov, S. Yakunin, F. Krumeich, N. P. Stadie, M. V. Kovalenko, *Nano Lett.* **2016**, *16*, 5866.
[72] Q. A. Akkerman, G. Rainò, M. V. Kovalenko, L. Manna, *Nat. Mater.* **2018**, *17*, 394.
[73] S. ten Brinck, I. Infante, *ACS Energy Lett.* **2016**, *1*, 1266.
[74] Z. Zheng, O. M. Awartani, B. Gautam, D. Liu, Y. Qin, W. Li, A. Bataller, K. Gundogdu, H. Ade, J. Hou, *Adv. Mater.* **2017**, *29*, 1604241.

© 2021 Wiley-VCH GmbH

[75] H. Huang, M. I. Bodnarchuk, S. V. Kershaw, M. V. Kovalenko, A. L. Rogach, *ACS Energy Lett.* **2017**, *2*, 2071.
[76] M. V. Kovalenko, L. Protesescu, M. I. Bodnarchuk, *Science* **2017**, *358*, 745.
[77] Q. A. Akkerman, M. Gandini, F. Di Stasio, P. Rastogi, F. Palazon, G. Bertoni, J. M. Ball, M. Prato, A. Petrozza, L. Manna, *Nat. Energy* **2016**, *2*, 16194.
[78] M. de Jong, W. Chen, T. Angsten, A. Jain, R. Notestine, A. Gamst, M. Sluiter, C. K. Ande, S. van der Zwaag, J. J. Plata, C. Toher, S. Curtarolo, G. Ceder, K. A. Persson, M. Asta, *Sci. Data* **2015**, *2*, 150009.
[79] P. Wang, J. Guan, D. T. K. Galeschuk, Y. Yao, C. F. He, S. Jiang, S. Zhang, Y. Liu, M. Jin, C. Jin, Y. Song, *J. Phys. Chem. Lett.* **2017**, *8*, 2119.
[80] P. Roy, N. K. Sinha, S. Tiwari, A. Khare, *Sol. Energy* **2020**, *198*, 665.
[81] O. López-Rojas, J. G. Guzmán, presented at *2019 IEEE International Conference on Engineering Veracruz (ICEV)*, Boca del Rio, Mexico, October **2019**.
[82] W.-J. Yin, T. Shi, Y. Yan, *J. Phys. Chem. C* **2015**, *119*, 5253.
[83] Z. Xiao, W. Meng, J. Wang, D. B. Mitzi, Y. Yan, *Mater. Horiz.* **2017**, *4*, 206.
[84] W.-J. Yin, T. Shi, Y. Yan, *Adv. Mater.* **2014**, *26*, 4653.
[85] H. Wei, D. Li, X. Zheng, Q. Meng, *Chin. Phys. B* **2018**, *27*, 018808.
[86] F. Zhou, Z. Li, H. Chen, Q. Wang, L. Ding, Z. Jin, *Nano Energy* **2020**, *73*, 104757.
[87] A. O. El-Ballouli, O. M. Bakr, O. F. Mohammed, *Chem. Mater.* **2019**, *31*, 6387.
[88] X. Wang, *Front. Optoelectron.* **2015**, *8*, 241.
[89] G. H. Carey, A. L. Abdelhady, Z. Ning, S. M. Thon, O. M. Bakr, E. H. Sargent, *Chem. Rev.* **2015**, *115*, 12732.
[90] S. Wang, C. Bi, A. Portniagin, J. Yuan, J. Ning, X. Xiao, X. Zhang, Y. Y. Li, S. V. Kershaw, J. Tian, A. L. Rogach, *ACS Energy Lett.* **2020**, *5*, 2401.
[91] T. Takagahara, K. Takeda, *Phys. Rev. B* **1992**, *46*, 15578.
[92] M. Thambidurai, N. Muthukumarasamy, S. Agilan, N. Murugan, S. Vasantha, R. Balasundaraprabhu, T. S. Senthil, *J. Mater. Sci.* **2010**, *45*, 3254.
[93] Y. Zhang, Y. Li, Y. Liu, H. Li, J. Fan, *Appl. Surf. Sci.* **2019**, *466*, 119.
[94] C.-H. M. Chuang, P. R. Brown, V. Bulović, M. G. Bawendi, *Nat. Mater.* **2014**, *13*, 796.
[95] S. Schmitt-Rink, D. A. B. Miller, D. S. Chemla, *Phys. Rev. B* **1987**, *35*, 8113.
[96] D. M. Kroupa, D. H. Arias, J. L. Blackburn, G. M. Carroll, D. B. Granger, J. E. Anthony, M. C. Beard, J. C. Johnson, *Nano Lett.* **2018**, *18*, 865.
[97] A. El-Ballouli, E. Alarousu, M. Bernardi, S. M. Aly, A. P. Lagrow, O. M. Bakr, O. F. Mohammed, *J. Am. Chem. Soc.* **2014**, *136*, 6952.
[98] L. Protesescu, S. Yakunin, M. I. Bodnarchuk, F. Krieg, R. Caputo, C. H. Hendon, R. X. Yang, A. Walsh, M. V. Kovalenko, *Nano Lett.* **2015**, *15*, 3692.
[99] C. R. Kagan, C. B. Murray, *Nat. Nanotechnol.* **2015**, *10*, 1013.
[100] M. A. Hines, G. D. Scholes, *Adv. Mater.* **2003**, *15*, 1844.
[101] M. C. Weidman, M. E. Beck, R. S. Hoffman, F. Prins, W. A. Tisdale, *ACS Nano* **2014**, *8*, 6363.
[102] J. Akhtar, M. Afzaal, M. Banski, A. Podhorodecki, M. Syperek, J. Misiewicz, U. Bangert, S. J. O. Hardman, D. M. Graham, W. R. Flavell, D. J. Binks, S. Gardonio, P. O'Brien, *J. Am. Chem. Soc.* **2011**, *133*, 5602.
[103] D. K. Smith, J. M. Luther, O. E. Semonin, A. J. Nozik, M. C. Beard, *ACS Nano* **2011**, *5*, 183.
[104] W. Ma, J. M. Luther, H. Zheng, Y. Wu, A. P. Alivisatos, *Nano Lett.* **2009**, *9*, 1699.
[105] Y.-H. Kim, C. Wolf, Y.-T. Kim, H. Cho, W. Kwon, S. Do, A. Sadhanala, C. G. Park, S.-W. Rhee, S. H. Im, R. H. Friend, T.-W. Lee, *ACS Nano* **2017**, *11*, 6586.
[106] J. Butkus, P. Vashishtha, K. Chen, J. K. Gallaher, S. K. K. Prasad, D. Z. Metin, G. Laufersky, N. Gaston, J. E. Halpert, J. M. Hodgkiss, *Chem. Mater.* **2017**, *29*, 3644.
[107] M. L. Böhm, T. C. Jellicoe, J. P. H. Rivett, A. Sadhanala, N. J. L. K. Davis, F. S. F. Morgenstern, K. C. Gödel, J. Govindasamy, C. G. M. Benson, N. C. Greenham, B. Ehrler, *J. Phys. Chem. Lett.* **2015**, *6*, 3510.
[108] J. Pan, L. N. Quan, Y. Zhao, W. Peng, B. Murali, S. P. Sarmah, M. Yuan, L. Sinatra, N. M. Alyami, J. Liu, E. Yassitepe, Z. Yang, O. Voznyy, R. Comin, M. N. Hedhili, O. F. Mohammed, Z. H. Lu, D. H. Kim, E. H. Sargent, O. M. Bakr, *Adv. Mater.* **2016**, *28*, 8718.
[109] A. Wang, Z. Jin, M. Cheng, F. Hao, L. Ding, *J. Energy Chem.* **2021**, *52*, 351.
[110] C. Yan, K. Lin, J. Lu, Z. Wei, *Front. Optoelectron.* **2020**, *13*, 282.
[111] F. Zhang, H. Zhong, C. Chen, X.-g. Wu, X. Hu, H. Huang, J. Han, B. Zou, Y. Dong, *ACS Nano* **2015**, *9*, 4533.
[112] I. Levchuk, A. Osvet, X. Tang, M. Brandl, J. D. Perea, F. Hoegl, G. J. Matt, R. Hock, M. Batentschuk, C. J. Brabec, *Nano Lett.* **2017**, *17*, 2765.
[113] M. Liu, G. Zhong, Y. Yin, J. Miao, K. Li, C. Wang, X. Xu, C. Shen, H. Meng, *Adv. Sci.* **2017**, *4*, 1700335.
[114] Z. Ning, D. Zhitomirsky, V. Adinolfi, B. Sutherland, J. Xu, O. Voznyy, P. Maraghechi, X. Lan, S. Hoogland, Y. Ren, E. H. Sargent, *Adv. Mater.* **2013**, *25*, 1719.
[115] J. N. Arenas, A. Soosaimanickam, H. P. Adl, R. Abargues, P. P. Boix, P. J. Rodríguez-Cantó, J. P. Martínez-Pastor, *Nanomaterials* **2020**, *10*, 1297.
[116] G. Ou, P. Fan, X. Ke, Y. Xu, K. Huang, H. Wei, W. Yu, H. Zhang, M. Zhong, H. Wu, Y. Li, *Nano Res.* **2018**, *11*, 751.
[117] R. Loef, A. J. Houtepen, E. Talgorn, J. Schoonman, A. Goossens, *Nano Lett.* **2009**, *9*, 856.
[118] L. Zhang, L. Yin, C. Wang, N. lun, Y. Qi, D. Xiang, *J. Phys. Chem. C* **2010**, *114*, 9651.
[119] S.-Y. Wu, H.-M. Zhang, P. Xu, S.-X. Zhang, *Spectrochim. Acta, Part A* **2010**, *75*, 230.
[120] A. Walsh, *J. Phys. Chem. Lett.* **2010**, *1*, 1284.
[121] D. Zherebetskyy, Y. Zhang, M. Salmeron, L.-W. Wang, *J. Phys. Chem. Lett.* **2015**, *6*, 4711.
[122] T. Fukuda, A. Takahashi, K. Takahira, H. Wang, T. Kubo, H. Segawa, *Sol. Energy Mater. Sol. Cells* **2019**, *195*, 220.
[123] X. Yang, J. Yang, J. Khan, H. Deng, S. Yuan, J. Zhang, Y. Xia, F. Deng, X. Zhou, F. Umar, Z. Jin, H. Song, C. Cheng, M. Sabry, J. Tang, *Nano-Micro Lett.* **2020**, *12*, 37.
[124] G. S. Shanker, A. Swarnkar, A. Chatterjee, S. Chakraborty, M. Phukan, N. Parveen, K. Biswas, A. Nag, *Nanoscale* **2015**, *7*, 9204.
[125] Z. Jin, A. Wang, Q. Zhou, Y. Wang, J. Wang, *Sci. Rep.* **2016**, *6*, 37106.
[126] S. Zang, Y. Wang, W. Su, H. Zhu, G. Li, X. Zhang, Y. Liu, *Phys. Status Solidi RRL* **2016**, *10*, 745.
[127] Y. Cao, A. Stavrinadis, T. Lasanta, D. So, G. Konstantatos, *Nat. Energy* **2016**, *1*, 16035.
[128] J. Kang, L.-W. Wang, *J. Phys. Chem. Lett.* **2017**, *8*, 489.
[129] H. Zhu, K. Miyata, Y. Fu, J. Wang, P. P. Joshi, D. Niesner, K. W. Williams, S. Jin, X.-Y. Zhu, *Science* **2016**, *353*, 1409.
[130] W. Shockley, H. J. Queisser, *J. Appl. Phys.* **1961**, *32*, 510.
[131] R. D. Schaller, V. I. Klimov, *Phys. Rev. Lett.* **2004**, *92*, 186601.
[132] V. I. Klimov, presented at *2008 Conference on Lasers and Electro-Optics and 2008 Conference on Quantum Electronics and Laser Science*, San Jose, California, USA, May **2008**.
[133] R. J. Ellingson, M. C. Beard, J. C. Johnson, P. Yu, O. I. Micic, A. J. Nozik, A. Shabaev, A. L. Efros, *Nano Lett.* **2005**, *5*, 865.
[134] A. J. Nozik, M. C. Beard, J. M. Luther, M. Law, R. J. Ellingson, J. C. Johnson, *Chem. Rev.* **2010**, *110*, 6873.
[135] V. I. Klimov, *Appl. Phys. Lett.* **2006**, *89*, 123118.
[136] M. C. Hanna, M. C. Beard, A. J. Nozik, *J. Phys. Chem. Lett.* **2012**, *3*, 2857.

© 2021 Wiley-VCH GmbH

[137] V. Sukhovatkin, S. Hinds, L. Brzozowski, E. H. Sargent, *Science* **2009**, *324*, 1542.
[138] O. E. Semonin, J. M. Luther, S. Choi, H.-Y. Chen, J. Gao, A. J. Nozik, M. C. Beard, *Science* **2011**, *334*, 1530.
[139] Z. Fang, M. Shang, X. Hou, Y. Zheng, Z. Du, Z. Yang, K.-C. Chou, W. Yang, Z. L. Wang, Y. Yang, *Nano Energy* **2019**, *61*, 389.
[140] C. de Weerd, L. Gomez, A. Capretti, D. M. Lebrun, E. Matsubara, J. Lin, M. Ashida, F. C. M. Spoor, L. D. A. Siebbeles, A. J. Houtepen, K. Suenaga, Y. Fujiwara, T. Gregorkiewicz, *Nat. Commun.* **2018**, *9*, 4199.
[141] I. Moreels, Y. Justo, B. De Geyter, K. Haustraete, J. C. Martins, Z. Hens, *ACS Nano* **2011**, *5*, 2004.
[142] D. J. Milliron, *Nat. Mater.* **2014**, *13*, 772.
[143] K. Chen, Q. Zhong, W. Chen, B. Sang, Y. Wang, T. Yang, Y. Liu, Y. Zhang, H. Zhang, *Adv. Funct. Mater.* **2019**, *29*, 1900991.
[144] J. Khan, X. Zhang, J. Yuan, Y. Wang, G. Shi, R. Patterson, J. Shi, X. Ling, L. Hu, T. Wu, S. Dai, W. Ma, *ACS Energy Lett.* **2020**, *5*, 3322.
[145] Y. Wang, J. Yuan, X. Zhang, X. Ling, B. W. Larson, Q. Zhao, Y. Yang, Y. Shi, J. M. Luther, W. Ma, *Adv. Mater.* **2020**, *32*, 2000449.
[146] L. Tan, P. Li, B. Sun, M. Chaker, D. Ma, *ACS Energy Lett.* **2017**, *2*, 1573.
[147] Y. Liu, G. Shi, Z. Liu, W. Ma, *Nanoscale Horiz.* **2021**, *6*, 8.
[148] T. Kim, S. Lim, S. Yun, S. Jeong, T. Park, J. Choi, *Small* **2020**, *16*, 2002460.
[149] A. Shrestha, M. Batmunkh, A. Tricoli, S. Z. Qiao, S. Dai, *Angew. Chem.* **2019**, *58*, 5202.
[150] J. H. Song, S. Jeong, *Nano Convergence* **2017**, *4*, 21.
[151] E. J. D. Klem, H. Shukla, S. Hinds, D. D. MacNeil, L. Levina, E. H. Sargent, *Appl. Phys. Lett.* **2008**, *92*, 212105.
[152] Y. Liu, M. Gibbs, J. Puthussery, S. Gaik, R. Ihly, H. W. Hillhouse, M. Law, *Nano Lett.* **2010**, *10*, 1960.
[153] A. H. Ip, S. M. Thon, S. Hoogland, O. Voznyy, D. Zhitomirsky, R. Debnath, L. Levina, L. R. Rollny, G. H. Carey, A. Fischer, K. W. Kemp, I. J. Kramer, Z. Ning, A. J. Labelle, K. W. Chou, A. Amassian, E. H. Sargent, *Nat. Nanotechnol.* **2012**, *7*, 577.
[154] X. Zheng, S. Yuan, J. Liu, J. Yin, F. Yuan, W.-S. Shen, K. Yao, M. Wei, C. Zhou, K. Song, B.-B. Zhang, Y. Lin, M. N. Hedhili, N. Wehbe, Y. Han, H.-T. Sun, Z.-H. Lu, T. D. Anthopoulos, O. F. Mohammed, E. H. Sargent, L.-S. Liao, O. M. Bakr, *ACS Energy Lett.* **2020**, *5*, 793.
[155] Z. Ning, O. Voznyy, J. Pan, S. Hoogland, V. Adinolfi, J. Xu, M. Li, A. R. Kirmani, J.-P. Sun, J. Minor, K. W. Kemp, H. Dong, L. Rollny, A. Labelle, G. Carey, B. Sutherland, I. Hill, A. Amassian, H. Liu, J. Tang, O. M. Bakr, E. H. Sargent, *Nat. Mater.* **2014**, *13*, 822.
[156] L. M. Wheeler, E. M. Sanehira, A. R. Marshall, P. Schulz, M. Suri, N. C. Anderson, J. A. Christians, D. Nordlund, D. Sokaras, T. Kroll, S. P. Harvey, J. J. Berry, L. Y. Lin, J. M. Luther, *J. Am. Chem. Soc.* **2018**, *140*, 10504.
[157] Q. Wang, Z. Jin, D. Chen, D. Bai, H. Bian, J. Sun, G. Zhu, G. Wang, S. Liu, *Adv. Energy Mater.* **2018**, *8*, 1800007.
[158] J. Kim, B. Koo, W. H. Kim, J. Choi, C. Choi, S. J. Lim, J.-S. Lee, D.-H. Kim, M. J. Ko, Y. Kim, *Nano Energy* **2019**, *66*, 104130.
[159] X. Ling, J. Yuan, X. Zhang, Y. Qian, S. M. Zakeeruddin, B. W. Larson, Q. Zhao, J. Shi, J. Yang, K. Ji, Y. Zhang, Y. Wang, C. Zhang, S. Duhm, J. M. Luther, M. Grätzel, W. Ma, *Adv. Mater.* **2020**, *32*, 2001906.
[160] X. Ling, S. Zhou, J. Yuan, J. Shi, Y. Qian, B. W. Larson, Q. Zhao, C. Qin, F. Li, G. Shi, C. Stewart, J. Hu, X. Zhang, J. M. Luther, S. Duhm, W. Ma, *Adv. Energy Mater.* **2019**, *9*, 1900721.
[161] J. Shi, F. Li, Y. Jin, C. Liu, B. Cohen-Kleinstein, S. Yuan, Y. Li, Z.-K. Wang, J. Yuan, W. Ma, *Angew. Chem.* **2020**, *59*, 22230.
[162] X. Zhang, D. Jia, C. Hägglund, V. A. Öberg, J. Du, J. Liu, E. M. J. Johansson, *Nano Energy* **2018**, *53*, 373.
[163] M. Gu, Y. Wang, F. Yang, K. Lu, Y. Xue, T. Wu, H. Fang, S. Zhou, Y. Zhang, X. Ling, Y. Xu, F. Li, J. Yuan, M. A. Loi, Z. Liu, W. Ma, *J. Mater. Chem. A* **2019**, *7*, 15951.
[164] D. S. Chung, J.-S. Lee, J. Huang, A. Nag, S. Ithurria, D. V. Talapin, *Nano Lett.* **2012**, *12*, 1813.
[165] J. Xu, O. Voznyy, M. Liu, A. R. Kirmani, G. Walters, R. Munir, M. Abdelsamie, A. H. Proppe, A. Sarkar, F. P. G. de Arquer, M. Wei, B. Sun, M. Liu, O. Ouellette, R. Quintero-Bermudez, J. Li, J. Fan, L. Quan, P. Todorovic, H. Tan, S. Hoogland, S. O. Kelley, M. Stefik, A. Amassian, E. H. Sargent, *Nat. Nanotechnol.* **2018**, *13*, 456.
[166] A. R. Kirmani, J. M. Luther, M. Abolhasani, A. Amassian, *ACS Energy Lett.* **2020**, *5*, 3069.
[167] Z. Ning, H. Dong, Q. Zhang, O. Voznyy, E. H. Sargent, *ACS Nano* **2014**, *8*, 10321.
[168] M. Liu, O. Voznyy, R. Sabatini, F. P. G. de Arquer, R. Munir, A. H. Balawi, X. Lan, F. Fan, G. Walters, A. R. Kirmani, S. Hoogland, F. Laquai, A. Amassian, E. H. Sargent, *Nat. Mater.* **2017**, *16*, 258.
[169] K. W. Johnston, A. G. Pattantyus-Abraham, J. P. Clifford, S. H. Myrskog, D. D. MacNeil, L. Levina, E. H. Sargent, *Appl. Phys. Lett.* **2008**, *92*, 151115.
[170] J. M. Luther, M. Law, M. C. Beard, Q. Song, M. O. Reese, R. J. Ellingson, A. J. Nozik, *Nano Lett.* **2008**, *8*, 3488.
[171] C. Piliego, L. Protesescu, S. Z. Bisri, M. V. Kovalenko, M. A. Loi, *Energy Environ. Sci.* **2013**, *6*, 3054.
[172] A. G. Pattantyus-Abraham, I. J. Kramer, A. R. Barkhouse, X. Wang, G. Konstantatos, R. Debnath, L. Levina, I. Raabe, M. K. Nazeeruddin, M. Grätzel, E. H. Sargent, *ACS Nano* **2010**, *4*, 3374.
[173] L. Hu, D.-B. Li, L. Gao, H. Tan, C. Chen, K. Li, M. Li, J.-B. Han, H. Song, H. Liu, J. Tang, *Adv. Funct. Mater.* **2016**, *26*, 1899.
[174] H. Liu, J. Tang, I. J. Kramer, R. Debnath, G. I. Koleilat, X. Wang, A. Fisher, R. Li, L. Brzozowski, L. Levina, E. H. Sargent, *Adv. Mater.* **2011**, *23*, 3832.
[175] B. Ehrler, K. P. Musselman, M. L. Böhm, F. S. F. Morgenstern, Y. Vaynzof, B. J. Walker, J. L. MacManus-Driscoll, N. C. Greenham, *ACS Nano* **2013**, *7*, 4210.
[176] A. J. Labelle, S. M. Thon, S. Masala, M. M. Adachi, H. Dong, M. Farahani, A. H. Ip, A. Fratalocchi, E. H. Sargent, *Nano Lett.* **2015**, *15*, 1101.
[177] J. Tang, H. Liu, D. Zhitomirsky, S. Hoogland, X. Wang, M. Furukawa, L. Levina, E. H. Sargent, *Nano Lett.* **2012**, *12*, 4889.
[178] Z. Jin, M. Yuan, H. Li, H. Yang, Q. Zhou, H. Liu, X. Lan, M. Liu, J. Wang, E. H. Sargent, Y. Li, *Adv. Funct. Mater.* **2016**, *26*, 5284.
[179] K. Lu, Y. Wang, Z. Liu, L. Han, G. Shi, H. Fang, J. Chen, X. Ye, S. Chen, F. Yang, A. G. Shulga, T. Wu, M. Gu, S. Zhou, J. Fan, M. A. Loi, W. Ma, *Adv. Mater.* **2018**, *30*, 1707572.
[180] Y. Xue, F. Yang, J. Yuan, Y. Zhang, M. Gu, Y. Xu, X. Ling, Y. Wang, F. Li, T. Zhai, J. Li, C. Cui, Y. Chen, W. Ma, *ACS Energy Lett.* **2019**, *4*, 2850.
[181] H. Aqoma, S.-Y. Jang, *Energy Environ. Sci.* **2018**, *11*, 1603.
[182] G. Yang, Y. Zhu, J. Huang, X. Xu, S. Cui, Z. Lu, *Opt. Express* **2019**, *27*, A1338.
[183] M. A. Mubarok, F. T. A. Wibowo, H. Aqoma, N. Vamsi Krishna, W. Lee, D. Y. Ryu, S. Cho, I. H. Jung, S.-Y. Jang, *ACS Energy Lett.* **2020**, *5*, 3452.
[184] M. A. Mubarok, H. Aqoma, F. T. A. Wibowo, W. Lee, H. M. Kim, D. Y. Ryu, J.-W. Jeon, S.-Y. Jang, *Adv. Energy Mater.* **2020**, *10*, 1902933.
[185] H. I. Kim, J. Lee, M.-J. Choi, S. U. Ryu, K. Choi, S. Lee, S. Hoogland, F. P. G. de Arquer, E. H. Sargent, T. Park, *Adv. Energy Mater.* **2020**, *10*, 2002084.
[186] H. D. Pham, T. C.-J. Yang, S. M. Jain, G. J. Wilson, P. Sonar, *Adv. Energy Mater.* **2020**, *10*, 1903326.
[187] A. K. Jena, Y. Numata, M. Ikegami, T. Miyasaka, *J. Mater. Chem. A* **2018**, *6*, 2219.
[188] A. Pellaroque, N. K. Noel, S. N. Habisreutinger, Y. Zhang, S. Barlow, S. R. Marder, H. J. Snaith, *ACS Energy Lett.* **2017**, *2*, 2044.
[189] H. J. Snaith, M. Grätzel, *Appl. Phys. Lett.* **2006**, *89*, 262114.

© 2021 Wiley-VCH GmbH

[190] H. D. Pham, T. T. Do, J. Kim, C. Charbonneau, S. Manzhos, K. Feron, W. C. Tsoi, J. R. Durrant, S. M. Jain, P. Sonar, *Adv. Energy Mater.* **2018**, *8*, 1703007.
[191] J. Shi, F. Li, J. Yuan, X. Ling, S. Zhou, Y. Qian, W. Ma, *J. Mater. Chem. A* **2019**, *7*, 20936.
[192] Y. Kim, E. H. Jung, G. Kim, D. Kim, B. J. Kim, J. Seo, *Adv. Energy Mater.* **2018**, *8*, 1801668.
[193] T. Liu, K. Chen, Q. Hu, R. Zhu, Q. Gong, *Adv. Energy Mater.* **2016**, *6*, 1600457.
[194] C. Xiao, Q. Zhao, C.-S. Jiang, Y. Sun, M. M. Al-Jassim, S. U. Nanayakkara, J. M. Luther, *Nano Energy* **2020**, *78*, 105319.
[195] S. B. Shivarudraiah, M. Ng, C. H. A. Li, J. E. Halpert, *ACS Appl. Energy Mater.* **2020**, *3*, 5620.
[196] Q. Zhao, A. Hazarika, X. Chen, S. P. Harvey, B. W. Larson, G. R. Teeter, J. Liu, T. Song, C. Xiao, L. Shaw, M. Zhang, G. Li, M. C. Beard, J. M. Luther, *Nat. Commun.* **2019**, *10*, 2842.
[197] X. Wang, G. I. Koleilat, J. Tang, H. Liu, I. J. Kramer, R. Debnath, L. Brzozowski, D. A. R. Barkhouse, L. Levina, S. Hoogland, E. H. Sargent, *Nat. Photonics* **2011**, *5*, 480.
[198] Y. Gao, J. Zheng, W. Chen, L. Yuan, Z. L. Teh, J. Yang, X. Cui, G. Conibeer, R. Patterson, S. Huang, *J. Phys. Chem. Lett.* **2019**, *10*, 5729.
[199] Y. Zhang, M. Gu, N. Li, Y. Xu, X. Ling, Y. Wang, S. Zhou, F. Li, F. Yang, K. Ji, J. Yuan, W. Ma, *J. Mater. Chem. A* **2018**, *6*, 24693.
[200] F. Qiao, Y. Xie, Z. Weng, H. Chu, *J. Energy Chem.* **2020**, *50*, 230.
[201] A. Karani, L. Yang, S. Bai, M. H. Futscher, H. J. Snaith, B. Ehrler, N. C. Greenham, D. Di, *ACS Energy Lett.* **2018**, *3*, 869.
[202] H. Aqoma, I. F. Imran, M. A. Mubarok, W. T. Hadmojo, Y. R. Do, S.-Y. Jang, *Adv. Energy Mater.* **2020**, *10*, 1903294.
[203] A. Manekkathodi, B. Chen, J. Kim, S.-W. Baek, B. Scheffel, Y. Hou, O. Ouellette, M. I. Saidaminov, O. Voznyy, V. E. Madhavan, A. Belaidi, S. Ashhab, E. Sargent, *J. Mater. Chem. A* **2019**, *7*, 26020.
[204] G. Shi, Y. Wang, Z. Liu, L. Han, J. Liu, Y. Wang, K. Lu, S. Chen, X. Ling, Y. Li, S. Cheng, W. Ma, *Adv. Energy Mater.* **2017**, *7*, 1602667.
[205] H. I. Kim, S.-W. Baek, M.-J. Choi, B. Chen, O. Ouellette, K. Choi, B. Scheffel, H. Choi, M. Biondi, S. Hoogland, F. P. G. de Arquer, T. Park, E. H. Sargent, *Adv. Mater.* **2020**, *32*, 2004657.
[206] M. M. Tavakoli, M. Nasilowski, J. Zhao, M. G. Bawendi, J. Kong, *Small* **2019**, *3*, 1900449.
[207] J. M. Luther, J. Gao, M. T. Lloyd, O. E. Semonin, M. C. Beard, A. J. Nozik, *Adv. Mater.* **2010**, *22*, 3704.
[208] R. Debnath, M. T. Greiner, I. J. Kramer, A. Fischer, J. Tang, D. A. R. Barkhouse, X. Wang, L. Levina, Z.-H. Lu, E. H. Sargent, *Appl. Phys. Lett.* **2010**, *97*, 023109.
[209] D. A. R. Barkhouse, R. Debnath, I. J. Kramer, D. Zhitomirsky, A. G. Pattantyus-Abraham, L. Levina, L. Etgar, M. Grätzel, E. H. Sargent, *Adv. Mater.* **2011**, *23*, 3134.
[210] J. Tang, K. W. Kemp, S. Hoogland, K. S. Jeong, H. Liu, L. Levina, M. Furukawa, X. Wang, R. Debnath, D. Cha, K. W. Chou, A. Fischer, A. Amassian, J. B. Asbury, E. H. Sargent, *Nat. Mater.* **2011**, *10*, 765.
[211] I. J. Kramer, D. Zhitomirsky, J. D. Bass, P. M. Rice, T. Topuria, L. Krupp, S. M. Thon, A. H. Ip, R. Debnath, H.-C. Kim, E. H. Sargent, *Adv. Mater.* **2012**, *24*, 2315.
[212] X. Lan, J. Bai, S. Masala, S. M. Thon, Y. Ren, I. J. Kramer, S. Hoogland, A. Simchi, G. I. Koleilat, D. Paz-Soldan, Z. Ning, A. J. Labelle, J. Y. Kim, G. Jabbour, E. H. Sargent, *Adv. Mater.* **2013**, *25*, 1769.
[213] P. Maraghechi, A. J. Labelle, A. R. Kirmani, X. Lan, M. M. Adachi, S. M. Thon, S. Hoogland, A. Lee, Z. Ning, A. Fischer, A. Amassian, E. H. Sargent, *ACS Nano* **2013**, *7*, 6111.
[214] A. R. Kirmani, G. H. Carey, M. Abdelsamie, B. Yan, D. Cha, L. R. Rollny, X. Cui, E. H. Sargent, A. Amassian, *Adv. Mater.* **2014**, *26*, 4717.
[215] R. W. Crisp, D. M. Kroupa, A. R. Marshall, E. M. Miller, J. Zhang, M. C. Beard, J. M. Luther, *Sci. Rep.* **2015**, *5*, 9945.
[216] Z. Yang, A. Janmohamed, X. Lan, F. P. G. de Arquer, O. Voznyy, E. Yassitepe, G.-H. Kim, Z. Ning, X. Gong, R. Comin, E. H. Sargent, *Nano Lett.* **2015**, *15*, 7539.
[217] M. J. Speirs, D. N. Dirin, M. Abdu-Aguye, D. M. Balazs, M. V. Kovalenko, M. A. Loi, *Energy Environ. Sci.* **2016**, *9*, 2916.
[218] R. Azmi, H. Aqoma, W. T. Hadmojo, J.-M. Yun, S. Yoon, K. Kim, Y. R. Do, S.-H. Oh, S.-Y. Jang, *Adv. Energy Mater.* **2016**, *6*, 1502146.
[219] R. Azmi, S.-H. Oh, S.-Y. Jang, *ACS Energy Lett.* **2016**, *1*, 100.
[220] X. Lan, O. Voznyy, F. P. G. de Arquer, M. Liu, J. Xu, A. H. Proppe, G. Walters, F. Fan, H. Tan, M. Liu, Z. Yang, S. Hoogland, E. H. Sargent, *Nano Lett.* **2016**, *16*, 4630.
[221] R. Azmi, S. Y. Nam, S. Sinaga, S.-H. Oh, T. K. Ahn, S. C. Yoon, I. H. Jung, S.-Y. Jang, *Nano Energy* **2017**, *39*, 355.
[222] J. Choi, Y. Kim, J. W. Jo, J. Kim, B. Sun, G. Walters, F. P. G. de Arquer, R. Quintero-Bermudez, Y. Li, C. S. Tan, L. N. Quan, A. P. T. Kam, S. Hoogland, Z. Lu, O. Voznyy, E. H. Sargent, *Adv. Mater.* **2017**, *29*, 1702350.
[223] J. W. Jo, Y. Kim, J. Choi, F. P. G. de Arquer, G. Walters, B. Sun, O. Ouellette, J. Kim, A. H. Proppe, R. Quintero-Bermudez, J. Fan, J. Xu, C. S. Tan, O. Voznyy, E. H. Sargent, *Adv. Mater.* **2017**, *29*, 1703627.
[224] A. Stavrinadis, S. Pradhan, P. Papagiorgis, G. Itskos, G. Konstantatos, *ACS Energy Lett.* **2017**, *2*, 739.
[225] Z. Yang, J. Z. Fan, A. H. Proppe, F. P. G. d. Arquer, D. Rossouw, O. Voznyy, X. Lan, M. Liu, G. Walters, R. Quintero-Bermudez, B. Sun, S. Hoogland, G. A. Botton, S. O. Kelley, E. H. Sargent, *Nat. Commun.* **2017**, *8*, 1325.
[226] X. Zhang, P. K. Santra, L. Tian, M. B. Johansson, H. Rensmo, E. M. J. Johansson, *ACS Nano* **2017**, *11*, 8478.
[227] R. Azmi, G. Seo, T. K. Ahn, S.-Y. Jang, *ACS Appl. Mater. Interfaces* **2018**, *10*, 35244.
[228] S.-W. Baek, S.-H. Lee, J. H. Song, C. Kim, Y.-S. Ha, H. Shin, H. Kim, S. Jeong, J.-Y. Lee, *Energy Environ. Sci.* **2018**, *11*, 2078.
[229] L. Hu, Z. Zhang, R. J. Patterson, Y. Hu, W. Chen, C. Chen, D. Li, C. Hu, C. Ge, Z. Chen, L. Yuan, C. Yan, N. Song, Z. L. Teh, G. J. Conibeer, J. Tang, S. Huang, *Nano Energy* **2018**, *46*, 212.
[230] J. Kim, O. Ouellette, O. Voznyy, M. Wei, J. Choi, M.-J. Choi, J. W. Jo, S.-W. Baek, J. Fan, M. I. Saidaminov, B. Sun, P. Li, D.-H. Nam, S. Hoogland, Z.-H. Lu, F. P. G. de Arquer, E. H. Sargent, *Adv. Mater.* **2018**, *30*, 1803830.
[231] L. Hu, X. Geng, S. Singh, J. Shi, Y. Hu, S. Li, X. Guan, T. He, X. Li, Z. Cheng, R. Patterson, S. Huang, T. Wu, *Nano Energy* **2019**, *64*, 103922.
[232] W. Ahmad, J. He, Z. Liu, K. Xu, Z. Chen, X. Yang, D. Li, Y. Xia, J. Zhang, C. Chen, *Adv. Mater.* **2019**, *31*, 1900593.
[233] M. Biondi, M.-J. Choi, O. Ouellette, S.-W. Baek, P. Todorović, B. Sun, S. Lee, M. Wei, P. Li, A. R. Kirmani, L. K. Sagar, L. J. Richter, S. Hoogland, Z.-H. Lu, F. P. G. de Arquer, E. H. Sargent, *Adv. Mater.* **2020**, *32*, 1906199.
[234] B. Sun, M. Vafaie, L. Levina, M. Wei, Y. Dong, Y. Gao, H. T. Kung, M. Biondi, A. H. Proppe, B. Chen, M.-J. Choi, L. K. Sagar, O. Voznyy, S. O. Kelley, F. Laquai, Z.-H. Lu, S. Hoogland, F. P. G. de Arquer, E. H. Sargent, *Nano Lett.* **2020**, *20*, 3694.
[235] J. Yuan, X. Ling, D. Yang, F. Li, S. Zhou, J. Shi, Y. Qian, J. Hu, Y. Sun, Y. Yang, X. Gao, S. Duhm, Q. Zhang, W. Ma, *Joule* **2018**, *2*, 2450.
[236] Q. Zeng, X. Zhang, X. Feng, S. Lu, Z. Chen, X. Yong, S. A. T. Redfern, H. Wei, H. Wang, H. Shen, W. Zhang, W. Zheng, H. Zhang, J. S. Tse, B. Yang, *Adv. Mater.* **2018**, *30*, 1705393.
[237] J. Xue, J.-W. Lee, Z. Dai, R. Wang, S. Nuryyeva, M. E. Liao, S.-Y. Chang, L. Meng, D. Meng, P. Sun, O. Lin, M. S. Goorsky, Y. Yang, *Joule* **2018**, *2*, 1866.
[238] F. Liu, C. Ding, Y. Zhang, T. Kamisaka, Q. Zhao, J. M. Luther, T. Toyoda, S. Hayase, T. Minemoto, K. Yoshino, B. Zhang, S. Dai, J. Jiang, S. Tao, Q. Shen, *Chem. Mater.* **2019**, *31*, 798.
[239] J. Xi, C. Piao, J. Byeon, J. Yoon, Z. Wu, M. Choi, *Adv. Energy Mater.* **2019**, *9*, 1901787.

© 2021 Wiley-VCH GmbH

[240] J. Xue, R. Wang, L. Chen, S. Nuryyeva, T.-H. Han, T. Huang, S. Tan, J. Zhu, M. Wang, Z.-K. Wang, C. Zhang, J.-W. Lee, Y. Yang, *Adv. Mater.* **2019**, *31*, 1900111.
[241] C. Ding, F. Liu, Y. Zhang, D. Hirotani, X. Rin, S. Hayase, T. Minemoto, T. Masuda, R. Wang, Q. Shen, *Nano Energy* **2020**, *67*, 104267.
[242] M. Suri, A. Hazarika, B. W. Larson, Q. Zhao, M. Vallés-Pelarda, T. D. Siegler, M. K. Abney, A. J. Ferguson, B. A. Korgel, J. M. Luther, *ACS Energy Lett.* **2019**, *4*, 1954.
[243] K. Chen, W. Jin, Y. Zhang, T. Yang, P. Reiss, Q. Zhong, U. Bach, Q. Li, Y. Wang, H. Zhang, Q. Bao, Y. Liu, *J. Am. Chem. Soc.* **2020**, *142*, 3775.
[244] J. Kim, S. Cho, F. Dinic, J. Choi, C. Choi, S. M. Jeong, J.-S. Lee, O. Voznyy, M. J. Ko, Y. Kim, *Nano Energy* **2020**, *75*, 104985.
[245] H. Huang, X. Li, S. Chen, B. Qiu, J. Du, L. Meng, Z. Zhang, C. Yang, Y. Li, *J. Mater. Chem. A* **2019**, *7*, 27423.
[246] G. W. Hwang, D. Kim, J. M. Cordero, M. W. B. Wilson, C.-H. M. Chuang, J. C. Grossman, M. G. Bawendi, *Adv. Mater.* **2015**, *27*, 4481.
[247] J. Tang, L. Brzozowski, D. A. R. Barkhouse, X. Wang, R. Debnath, R. Wolowiec, E. Palmiano, L. Levina, A. G. Pattantyus-Abraham, D. Jamakosmanovic, E. H. Sargent, *ACS Nano* **2010**, *4*, 869.
[248] S. Kim, S. H. Im, M. Kang, J. H. Heo, S. I. Seok, S.-W. Kim, I. Mora-Seró, J. Bisquert, *Phys. Chem. Chem. Phys.* **2012**, *14*, 14999.
[249] H. Lee, H.-J. Song, M. Shim, C. Lee, *Energy Environ. Sci.* **2020**, *13*, 404.
[250] J. Y. Woo, S. Lee, S. Lee, W. D. Kim, K. Lee, K. Kim, H. J. An, D. C. Lee, S. Jeong, *J. Am. Chem. Soc.* **2016**, *138*, 876.
[251] M. Sykora, A. Y. Koposov, J. A. McGuire, R. K. Schulze, O. Tretiak, J. M. Pietryga, V. I. Klimov, *ACS Nano* **2010**, *4*, 2021.
[252] K.-S. Cho, D. V. Talapin, W. Gaschler, C. B. Murray, *J. Am. Chem. Soc.* **2005**, *127*, 7140.
[253] L. Hu, Q. Lei, X. Guan, R. Patterson, J. Yuan, C.-H. Lin, J. Kim, X. Geng, A. Younis, X. Wu, X. Liu, T. Wan, D. Chu, T. Wu, S. Huang, *Adv. Sci.* **2021**, *8*, 2003138.
[254] B. Fritzinger, I. Moreels, P. Lommens, R. Koole, Z. Hens, J. C. Martins, *J. Am. Chem. Soc.* **2009**, *131*, 3024.
[255] H. Choi, J.-H. Ko, Y.-H. Kim, S. Jeong, *J. Am. Chem. Soc.* **2013**, *135*, 5278.
[256] F. A. Soria, E. M. Patrito, P. Paredes-Olivera, *J. Phys. Chem. C* **2012**, *116*, 24607.
[257] E. Yassitepe, Z. Yang, O. Voznyy, Y. Kim, G. Walters, J. A. Castañeda, P. Kanjanaboos, M. Yuan, X. Gong, F. Fan, J. Pan, S. Hoogland, R. Comin, O. M. Bakr, L. A. Padilha, A. F. Nogueira, E. H. Sargent, *Adv. Funct. Mater.* **2016**, *26*, 8757.
[258] J. B. Hoffman, G. Zaiats, I. Wappes, P. V. Kamat, *Chem. Mater.* **2017**, *29*, 9767.
[259] R. An, F. Zhang, X. Zou, Y. Tang, M. Liang, I. Oshchapovskyy, Y. Liu, A. Honarfar, Y. Zhong, C. Li, H. Geng, J. Chen, S. E. Canton, T. Pullerits, K. Zheng, *ACS Appl. Mater. Interfaces* **2018**, *10*, 39222.
[260] G. Almeida, I. Infante, L. Manna, *Science* **2019**, *364*, 833.
[261] J. Chen, D. Jia, E. M. J. Johansson, A. Hagfeldt, X. Zhang, *Energy Environ. Sci.* **2021**, *14*, 224.
[262] M. I. Asghar, J. Zhang, H. Wang, P. D. Lund, *Renewable Sustainable Energy Rev.* **2017**, *77*, 131.
[263] N. A. N. Ouedraogo, Y. Chen, Y. Y. Xiao, Q. Meng, C. B. Han, H. Yan, Y. Zhang, *Nano Energy* **2020**, *67*, 104249.
[264] D. Wang, M. Wright, N. K. Elumalai, A. Uddin, *Sol. Energy Mater. Sol. Cells* **2016**, *147*, 255.
[265] T. Leijtens, G. E. Eperon, N. K. Noel, S. N. Habisreutinger, A. Petrozza, H. J. Snaith, *Adv. Energy Mater.* **2015**, *5*, 1500963.
[266] Y. S. Kwon, J. Lim, H.-J. Yun, Y.-H. Kim, T. Park, *Energy Environ. Sci.* **2014**, *7*, 1454.
[267] J. Liu, Y. Wu, C. Qin, X. Yang, T. Yasuda, A. Islam, K. Zhang, W. Peng, W. Chen, L. Han, *Energy Environ. Sci.* **2014**, *7*, 2963.
[268] Y. Hu, T. Qiu, F. Bai, X. Miao, S. Zhang, *J. Mater. Chem. A* **2017**, *5*, 25258.
[269] N. Aristidou, I. Sanchez-Molina, T. Chotchuangchutchaval, M. Brown, L. Martinez, T. Rath, S. A. Haque, *Angew. Chem.* **2015**, *54*, 8208.
[270] Y. Rong, L. Liu, A. Mei, X. Li, H. Han, *Adv. Energy Mater.* **2015**, *5*, 1501066.
[271] G. Divitini, S. Cacovich, F. Matteocci, L. Cinà, A. Di Carlo, C. Ducati, *Nat. Energy* **2016**, *1*, 15012.
[272] R. J. Sutton, G. E. Eperon, L. Miranda, E. S. Parrott, B. A. Kamino, J. B. Patel, M. T. Hörantner, M. B. Johnston, A. A. Haghighirad, D. T. Moore, H. J. Snaith, *Adv. Energy Mater.* **2016**, *6*, 1502458.
[273] Y. Hu, F. Bai, X. Liu, Q. Ji, X. Miao, T. Qiu, S. Zhang, *ACS Energy Lett.* **2017**, *2*, 2219.
[274] T. Moot, D. R. Dikova, A. Hazarika, T. H. Schloemer, S. N. Habisreutinger, N. Leick, S. P. Dunfield, B. A. Rosales, S. P. Harvey, J. R. Pfeilsticker, G. Teeter, L. M. Wheeler, B. W. Larson, J. M. Luther, *Chem. Mater.* **2020**, *32*, 7850.
[275] C. Eames, J. M. Frost, P. R. F. Barnes, B. C. O'Regan, A. Walsh, M. S. Islam, *Nat. Commun.* **2015**, *6*, 7497.
[276] J. S. Yun, J. Seidel, J. Kim, A. M. Soufiani, S. Huang, J. Lau, N. J. Jeon, S. I. Seok, M. A. Green, A. Ho-Baillie, *Adv. Energy Mater.* **2016**, *6*, 1600330.
[277] J. M. Ball, A. Petrozza, *Nat. Energy* **2016**, *1*, 16149.
[278] J. M. Azpiroz, E. Mosconi, J. Bisquert, F. De Angelis, *Energy Environ. Sci.* **2015**, *8*, 2118.
[279] J.-N. Yang, Y. Song, J.-S. Yao, K.-H. Wang, J.-J. Wang, B.-S. Zhu, M.-M. Yao, S. U. Rahman, Y.-F. Lan, F.-J. Fan, H.-B. Yao, *J. Am. Chem. Soc.* **2020**, *142*, 2956.
[280] J. Kim, H. Jung, J. Song, K. Kim, C. Lee, *ACS Appl. Mater. Interfaces* **2017**, *9*, 24052.
[281] S. Lim, J. Kim, J. Y. Park, J. Min, S. Yun, T. Park, Y. Kim, J. Choi, *ACS Appl. Mater. Interfaces* **2021**, *13*, 6119.
[282] K. Domanski, J.-P. Correa-Baena, N. Mine, M. K. Nazeeruddin, A. Abate, M. Saliba, W. Tress, A. Hagfeldt, M. Grätzel, *ACS Nano* **2016**, *10*, 6306.
[283] N. Li, X. Niu, Q. Chen, H. Zhou, *Chem. Soc. Rev.* **2020**, *49*, 8235.
[284] Y.-C. Zhao, W.-K. Zhou, X. Zhou, K.-H. Liu, D.-P. Yu, Q. Zhao, *Light: Sci. Appl.* **2017**, *6*, e16243.
[285] D. H. Webber, R. L. Brutchey, *J. Am. Chem. Soc.* **2012**, *134*, 1085.
[286] C. Zheng, C. Bi, F. Huang, D. Binks, J. Tian, *ACS Appl. Mater. Interfaces* **2019**, *11*, 25410.
[287] J. M. Pietryga, D. J. Werder, D. J. Williams, J. L. Casson, R. D. Schaller, V. I. Klimov, J. A. Hollingsworth, *J. Am. Chem. Soc.* **2008**, *130*, 4879.
[288] J. Choi, M.-J. Choi, J. Kim, F. Dinic, P. Todorovic, B. Sun, M. Wei, S.-W. Baek, S. Hoogland, F. P. G. de Arquer, O. Voznyy, E. H. Sargent, *Adv. Mater.* **2020**, *32*, 1906497.
[289] H. Yu, Y. Lu, Z. Feng, Y. Wu, Z. Liu, P. Xia, J. Qian, Y. Chen, L. Liu, K. Cao, S. Chen, W. Huang, *Nanoscale* **2019**, *11*, 9103.
[290] K. Xu, E. T. Vickers, L. Rao, S. A. Lindley, A. L. C. Allen, B. Luo, X. Li, J. Z. Zhang, *Chem. - Eur. J.* **2019**, *25*, 5014.
[291] C. Zhang, B. Wang, Q. Wan, L. Kong, W. Zheng, Z. Li, L. Li, *Nanoscale* **2019**, *11*, 2602.
[292] N. J. Jeon, J. H. Noh, W. S. Yang, Y. C. Kim, S. Ryu, J. Seo, S. I. Seok, *Nature* **2015**, *517*, 476.
[293] T. Matsui, T. Yamamoto, T. Nishihara, R. Morisawa, T. Yokoyama, T. Sekiguchi, T. Negami, *Adv. Mater.* **2019**, *31*, 1806823.
[294] K. A. Bush, K. Frohna, R. Prasanna, R. E. Beal, T. Leijtens, S. A. Swifter, M. D. McGehee, *ACS Energy Lett.* **2018**, *3*, 428.
[295] W. J. Mir, A. Swarnkar, A. Nag, *Nanoscale* **2019**, *11*, 4278.
[296] Q. A. Akkerman, D. Meggiolaro, Z. Dang, F. De Angelis, L. Manna, *ACS Energy Lett.* **2017**, *2*, 2183.
[297] W. Liu, J. Zheng, M. Shang, Z. Fang, K.-C. Chou, W. Yang, X. Hou, T. Wu, *J. Mater. Chem. A* **2019**, *7*, 10912.
[298] S. Liu, L. Yuan, Y. Zhao, Y. Chen, W. Xiang, X. Liang, *J. Alloys Compd.* **2019**, *806*, 1022.

© 2021 Wiley-VCH GmbH

[299] L. Zhang, C. Kang, G. Zhang, Z. Pan, Z. Huang, S. Xu, H. Rao, H. Liu, S. Wu, X. Wu, X. Li, Z. Zhu, X. Zhong, A. K.-Y. Jen, *Adv. Funct. Mater.* **2021**, *31*, 2005930.
[300] H. Liu, D. Zhitomirsky, S. Hoogland, J. Tang, I. J. Kramer, Z. Ning, E. H. Sargent, *Appl. Phys. Lett.* **2012**, *101*, 151112.
[301] J. Chang, Y. Kuga, I. Mora-Seró, T. Toyoda, Y. Ogomi, S. Hayase, J. Bisquert, Q. Shen, *Nanoscale* **2015**, *7*, 5446.
[302] L. Duan, B. Sang, M. He, Y. Zhang, M. A. Hossain, M. H. Rahaman, Q. Wei, Y. Zou, A. Uddin, B. Hoex, *Sol. RRL* **2020**, *4*, 2000497.
[303] X. Zhang, C. Hägglund, E. M. J. Johansson, *Energy Environ. Sci.* **2017**, *10*, 216.
[304] M. V. Khenkin, E. A. Katz, A. Abate, G. Bardizza, J. J. Berry, C. Brabec, F. Brunetti, V. Bulović, Q. Burlingame, A. Di Carlo, R. Cheacharoen, Y.-B. Cheng, A. Colsmann, S. Cros, K. Domanski, M. Dusza, C. J. Fell, S. R. Forrest, Y. Galagan, D. Di Girolamo, M. Grätzel, A. Hagfeldt, E. von Hauff, H. Hoppe, J. Kettle, H. Köbler, M. S. Leite, S. Liu, Y.-L. Loo, J. M. Luther, et al., *Nat. Energy* **2020**, *5*, 35.
[305] J. M. Luther, J. Gao, M. T. Lloyd, O. E. Semonin, M. C. Beard, A. J. Nozik, *Adv. Mater.* **2010**, *22*, 3704.
[306] J. Tang, X. Wang, L. Brzozowski, D. A. R. Barkhouse, R. Debnath, L. Levina, E. H. Sargent, *Adv. Mater.* **2010**, *22*, 1398.
[307] M.-J. Choi, J. Oh, J.-K. Yoo, J. Choi, D. M. Sim, Y. S. Jung, *Energy Environ. Sci.* **2014**, *7*, 3052.
[308] X.-D. Mai, H. J. An, J. H. Song, J. Jang, S. Kim, S. Jeong, *J. Mater. Chem. A* **2014**, *2*, 20799.
[309] S. Kim, A. R. Marshall, D. M. Kroupa, E. M. Miller, J. M. Luther, S. Jeong, M. C. Beard, *ACS Nano* **2015**, *9*, 8157.
[310] Y. Zhang, C. Ding, G. Wu, N. Nakazawa, J. Chang, Y. Ogomi, T. Toyoda, S. Hayase, K. Katayama, Q. Shen, *J. Phys. Chem. C* **2016**, *120*, 28509.
[311] A. R. Kirmani, A. D. Sheikh, M. R. Niazi, M. A. Haque, M. Liu, F. P. G. de Arquer, J. Xu, B. Sun, O. Voznyy, N. Gasparini, D. Baran, T. Wu, E. H. Sargent, A. Amassian, *Adv. Mater.* **2018**, *30*, 1801661.
[312] F. Yang, Y. Xu, M. Gu, S. Zhou, Y. Wang, K. Lu, Z. Liu, X. Ling, Z. Zhu, J. Chen, Z. Wu, Y. Zhang, Y. Xue, F. Li, J. Yuan, W. Ma, *J. Mater. Chem. A* **2018**, *6*, 17688.
[313] H. T. Dastjerdi, R. Tavakoli, P. Yadav, D. Prochowicz, M. Saliba, M. M. Tavakoli, *ACS Appl. Mater. Interfaces* **2019**, *11*, 26047.
[314] T. Kim, Y. Gao, H. Hu, B. Yan, Z. Ning, L. K. Jagadamma, K. Zhao, A. R. Kirmani, J. Eid, M. M. Adachi, E. H. Sargent, P. M. Beaujuge, A. Amassian, *Nano Energy* **2015**, *17*, 196.
[315] S. M. Lee, T. Kumari, B. Lee, Y. Cho, J. Lee, J. Oh, M. Jeong, S. Jung, C. Yang, *Small* **2020**, *16*, 1905309.
[316] S. Zhou, Z. Liu, Y. Wang, K. Lu, F. Yang, M. Gu, Y. Xu, S. Chen, X. Ling, Y. Zhang, F. Li, J. Yuan, W. Ma, *J. Mater. Chem. C* **2019**, *7*, 1575.
[317] S. G. Kwon, T. Hyeon, *Small* **2011**, *7*, 2685.
[318] C. B. Murray, D. J. Norris, M. G. Bawendi, *J. Am. Chem. Soc.* **1993**, *115*, 8706.
[319] Y. Wang, Z. Liu, N. Huo, F. Li, M. Gu, X. Ling, Y. Zhang, K. Lu, L. Han, H. Fang, A. G. Shulga, Y. Xue, S. Zhou, F. Yang, X. Tang, J. Zheng, M. A. Loi, G. Konstantatos, W. Ma, *Nat. Commun.* **2019**, *10*, 5136.
[320] H. Choi, J.-G. Lee, X. D. Mai, M. C. Beard, S. S. Yoon, S. Jeong, *Sci. Rep.* **2017**, *7*, 622.
[321] M. Eita, A. Usman, A. El-Ballouli, E. Alarousu, O. M. Bakr, O. F. Mohammed, *Small* **2015**, *11*, 112.
[322] C. Jiang, Z. Zhong, B. Liu, Z. He, J. Zou, L. Wang, J. Wang, J. Peng, Y. Cao, *ACS Appl. Mater. Interfaces* **2016**, *8*, 26162.
[323] W. Ji, S. Liu, H. Zhang, R. Wang, W. Xie, H. Zhang, *ACS Photonics* **2017**, *4*, 1271.
[324] I. J. Kramer, G. Moreno-Bautista, J. C. Minor, D. Kopilovic, E. H. Sargent, *Appl. Phys. Lett.* **2014**, *105*, 163902.
[325] H. Li, K. Wu, J. Lim, H.-J. Song, V. I. Klimov, *Nat. Energy* **2016**, *1*, 16157.
[326] F. Giustino, H. J. Snaith, *ACS Energy Lett.* **2016**, *1*, 1233.
[327] D. Porotnikov, M. Zamkov, *J. Phys. Chem. C* **2020**, *124*, 21895.
[328] D. E. Lee, S. Y. Kim, H. W. Jang, *J. Korean Ceram. Soc.* **2020**, *57*, 455.
[329] S. Tamang, S. Lee, H. Choi, S. Jeong, *Chem. Mater.* **2016**, *28*, 8119.
[330] W. Liu, J.-S. Lee, D. V. Talapin, *J. Am. Chem. Soc.* **2013**, *135*, 1349.
[331] D. Franke, D. K. Harris, O. Chen, O. T. Bruns, J. A. Carr, M. W. B. Wilson, M. G. Bawendi, *Nat. Commun.* **2016**, *7*, 12749.
[332] Z. Shi, J. Guo, Y. Chen, Q. Li, Y. Pan, H. Zhang, Y. Xia, W. Huang, *Adv. Mater.* **2017**, *29*, 1605005.
[333] M. Chen, M.-G. Ju, A. D. Carl, Y. Zong, R. L. Grimm, J. Gu, X. C. Zeng, Y. Zhou, N. P. Padture, *Joule* **2018**, *2*, 558.
[334] F. Jiang, D. Yang, Y. Jiang, T. Liu, X. Zhao, Y. Ming, B. Luo, F. Qin, J. Fan, H. Han, L. Zhang, Y. Zhou, *J. Am. Chem. Soc.* **2018**, *140*, 1019.
[335] B. J. Moon, S. J. Kim, S. Lee, A. Lee, H. Lee, D. S. Lee, T.-W. Kim, S.-K. Lee, S. Bae, S. H. Lee, *Adv. Mater.* **2019**, *31*, 1901716.
[336] J. Sun, J. Yang, J. I. Lee, J. H. Cho, M. S. Kang, *J. Phys. Chem. Lett.* **2018**, *9*, 1573.
[337] M. Leng, Z. Chen, Y. Yang, Z. Li, K. Zeng, K. Li, G. Niu, Y. He, Q. Zhou, J. Tang, *Angew. Chem.* **2016**, *55*, 15012.
[338] F. Wang, X. Jiang, H. Chen, Y. Shang, H. Liu, J. Wei, W. Zhou, H. He, W. Liu, Z. Ning, *Joule* **2018**, *2*, 2732.

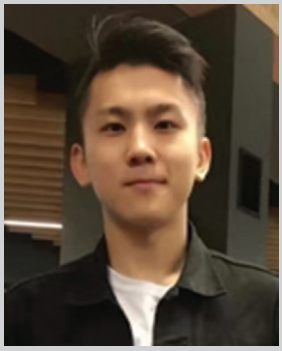

Leiping Duan is a visiting research fellow in the School of Material Science and Engineering, UNSW, and working on the high-efficiency thin-film solar cell. He received his Ph.D. degree and his master's degree in the School of Photovoltaic and Renewable Energy Engineering, University of New South Wales. His major research interests are perovskite organic solar cells, organic solar cells, tandem solar cells, semitransparent solar cells, and building integrated photovoltaic.

© 2021 Wiley-VCH GmbH

Long Hu is a Macquarie Research Fellow at School of Engineering, Macquarie University and a visiting Fellow in School of Materials Science and Engineering, University of New South Wales, Australia. In the past 9 years, he has been dedicated to fabricating highly efficiently and stable optoeleletronic devices based on the colloidal quantum dot such as PbS, PbSe, and halide perovskites.

Jianyu Yuan is an Associate Professor at Institute of Functional Nano and Soft Materials (FUNSOM), Soochow University. He received his Ph.D. degree from Soochow University in 2016. In 2014–2015, he worked at University of California, Santa Barbara (UCSB) as a joint Ph.D. student, and in summer 2018, he was a Visiting Professor at the National Renewable Energy Laboratory (NREL). Now his research interests include design and synthesis of semiconducting polymers, quantum dots, and hybrid systems for photovoltaic and other emerging optoelectronic application.

Tom Wu is as a Professor in School of Materials Science and Engineering, University of New South Wales (UNSW), Australia. He received Ph.D. degree from the University of Maryland, College Park in 2002. He worked as postdoc in Argonne National Laboratory in Chicago, assistant professor in Nanyang Technological University (NTU) Singapore, and associate professor in King Abdullah University of Science and Technology (KAUST) before joining UNSW. Dr. Wu works in the areas of oxide thin films, nanomaterials, and halide perovskites, with a focus on their electronic, magnetic, and optical functionalities.

© 2021 Wiley-VCH GmbH